Universidad de La Laguna

Facultad de Ciencias

Sección de Física

Caracterización de materiales ferroeléctricos: consideraciones sobre los ciclos de histéresis

Trabajo de Fin de Grado

Vicente Mendoza Afonso

Tutor: Manuel E. Torres

Julio 2023

Resumen

Este proyecto presenta un análisis integral de materiales ferroeléctricos a través de la investigación de ciclos de histéresis, densidad de corriente y el método Positive-Up-Negative-Down (PUND). El estudio tiene como objetivo diferenciar entre materiales ferroeléctricos propios, ferroeléctricos impropios y dieléctricos mediante la realización de mediciones a diferentes temperaturas y examinando sus comportamientos eléctricos bajo diversas condiciones externas.

La investigación parte de los compuestos iniciales, La_2O_3, Er_2O_3 y MoO_3. Se emplea el método de reacción en estado sólido para sintetizar $La_2(MoO_4)_3$ y $Er_2(MoO_4)_3$, los materiales base para posteriores modificaciones. Se logran tres proporciones diferentes de composiciones $La_{2-x}Er_x(MoO_4)_3$ ($x = 0.85$, 1 y 1.15) controlando cuidadosamente las cantidades de $La_2(MoO_4)_3$ y $Er_2(MoO_4)_3$ en la mezcla. Los polvos se muelen y mezclan a fondo para garantizar la homogeneidad, posteriormente se compactan en pastillas y se someten a tratamientos térmicos precisos.

Para permitir las mediciones eléctricas, se aplican electrodos de tintura de platino a las muestras. El uso de pintura de platino asegura un buen contacto eléctrico y minimiza posibles pérdidas en las mediciones. Las muestras se recubren con la pintura y, después de secarse, se someten a un proceso de tratamiento térmico. Este proceso implica colocar las muestras en un horno y calentarlas hasta 750°C, seguido de un enfriamiento rápido a temperatura ambiente. Este proceso garantiza la estabilidad y confiabilidad de la interfaz electrodo-material.

Se emplea el análisis de difracción de rayos X (XRD) para confirmar la formación de los materiales deseados. Los patrones de difracción se obtienen utilizando un difractómetro de rayos X de alta resolución, que proporciona información sobre la estructura cristalina y composición de fase de las muestras. Los picos de difracción se comparan con patrones de referencia para verificar la presencia de $La_2(MoO_4)_3$ y $Er_2(MoO_4)_3$ en las proporciones deseadas, confirmando el éxito del proceso de síntesis.

Los ciclos de histéresis se obtienen utilizando el sistema Radiant, un equipo especializado diseñado para mediciones precisas de histéresis. Las muestras se someten a la rutina de histéresis, que implica la aplicación de un campo eléctrico variable y la medición de la respuesta de polarización resultante. Los resultados de las mediciones de histéresis revelan perfiles distintos para las diferentes composiciones de La-Er. Las composiciones de $La_{0.85}Er_{1.15}(MoO_4)_3$ y $LaEr(MoO_4)_3$ exhiben un claro comportamiento ferroeléctrico a temperatura ambiente, con ciclos de histéresis bien definidos y capacidades significativas de conmutación de polarización. Sin embargo, $La_{1.15}Er_{0.85}(MoO_4)_3$ muestra un comportamiento ferroeléctrico menos pronunciado, indicando una reducción en las capacidades de conmutación de polarización.

Se realizan mediciones de densidad de corriente para estudiar la relación entre la densidad de corriente y el campo eléctrico aplicado. Esta técnica proporciona información sobre la conductividad eléctrica y la movilidad de portadores de carga de los materiales. Las mediciones se realizan por separado de la rutina de histéresis, lo que permite un análisis integral del comportamiento eléctrico. Los resultados de las mediciones de densidad de corriente brindan evidencia adicional de la naturaleza ferroeléctrica de las soluciones sólidas $La_{0.85}Er_{1.15}(MoO_4)_3$ y $LaEr(MoO_4)_3$, ya que muestran mayores densidades de corriente en comparación con los materiales ferroeléctricos impropios y dieléctricos.

Se emplea el método PUND para estudiar el comportamiento de conmutación de los materiales. Esta técnica implica la aplicación de una serie de pulsos de voltaje a las muestras y la medición de la respuesta de polarización resultante. Las mediciones de PUND brindan información valiosa sobre la dinámica de conmutación, la polarización remanente y el campo coercitivo de los materiales. Los resultados de las mediciones de PUND corroboran los hallazgos de los ciclos de histéresis, confirmando el comportamiento ferroeléctrico de las soluciones sólidas $La_{0.85}Er_{1.15}(MoO_4)_3$ y $LaEr(MoO_4)_3$.

Para validar las mediciones y proporcionar puntos de referencia, se incluyen materiales ferroeléctricos conocidos como PZT y $BaTiO_3$ como referencias ferroeléctricas. Además, se seleccionan materiales dieléctricos como Teflón y Al_2O_3 como puntos de comparación para el comportamiento

dieléctrico. La comparación con estos materiales de referencia mejora la comprensión de los datos medidos y valida las propiedades ferroeléctricas observadas en las soluciones sólidas con menor concentración de La: $La_{0.85}Er_{1.15}(MoO_4)_3$ y $LaEr(MoO_4)_3$.

Con este estudio se pretende contribuir, estableciendo algunas pautas, diferenciar entre 'ciclos de histéresis´ asociados a pérdidas dieléctricas en cualquier material, de los ciclos de histéresis asociados a un material ferroléctrico. Esta distinción es crucial para una correcta caracterización de los materiales y evita conclusiones erróneas sobre sus propiedades ferroeléctricas. Al combinar mediciones de ciclos de histéresis, densidad de corriente y el método PUND, se obtiene un enfoque integral que permite discernir con mayor precisión entre materiales ferroeléctricos propios, materiales ferroeléctricos impropios y materiales dieléctricos.

Abstract

This project presents a comprehensive analysis of ferroelectric materials through the investigation of hysteresis cycles, density of current, and the Positive-Up-Negative-Down (PUND) method. The study aims to differentiate between proper ferroelectric, improper ferroelectric, and dielectric materials by conducting measurements at different temperatures and examining their electrical behaviors under various external conditions.

The research parts from the initial compounds, La_2O_3, Er_2O3, and MoO_3. The solid-state reaction method is employed to synthesize $La_2(MoO_4)_3$ and $Er_2(MoO_4)_3$, the base materials for further modifications. Three different proportions of $La_{2-x}Er_x(MoO_4)_3$ compositions ($x = 0.85$, 1, and 1.15) are achieved by carefully controlling the amounts of $La_2(MoO_4)_3$ and $Er_2(MoO_4)_3$ in the mixture. The powders are thoroughly ground and mixed to ensure homogeneity, as they are later compressed into pellets and subjected to precise thermal treatments.

To enable electrical measurements, platinum paint electrodes are applied to the samples. The use of platinum paint ensures good electrical contact and minimizes potential leaks in the measurements. The samples are coated with the paint, and after drying, they are subjected to a thermal treatment process. The treatment involves placing the samples in an oven and heating them up to 750°C followed by rapid quenching to room temperature. This process ensures the stability and reliability of the electrode-material interface.

X-ray diffraction analysis is employed to confirm the formation of the desired materials. The XRD patterns are obtained using a high-resolution X-ray diffractometer, which provides information about the crystal structure and phase composition of the samples. The diffraction peaks are compared with reference patterns to verify the presence of $La_2(MoO_4)_3$ and $Er_2(MoO_4)_3$ in the desired proportions, confirming the success of the synthesis process.

The hysteresis cycles are obtained using the Radiant system, a specialized equipment designed for precise hysteresis measurements. The samples are subjected to the hysteresis routine, which involves applying a varying electric field and measuring the resulting polarization response. The results of the hysteresis measurements reveal distinct profiles for the different La-Er compositions. $La_{0.85}Er_{1.15}(MoO_4)_3$ and $LaEr(MoO_4)_3$ compositions exhibit clear ferroelectric behavior at room temperature, with well-defined hysteresis loops and significant polarization switching capabilities. However, $La_{1.15}Er_{0.85}(MoO_4)_3$ shows less pronounced ferroelectric behavior, indicating a reduction in polarization switching capabilities.

Density of current measurements are conducted to study the relationship between current density and the applied electric field. This technique provides insights into the electrical conductivity and charge carrier mobility of the materials. The measurements are performed separately from the hysteresis routine, allowing for a comprehensive analysis of the electrical behavior. The results of the density of current measurements provide further evidence of the ferroelectric nature of $La_{0.85}Er_{1.15}(MoO_4)_3$ and $LaEr(MoO_4)_3$ compositions, as they exhibit higher current densities compared to the improper ferroelectric and dielectric materials.

The PUND method is employed to study the switching behavior of the materials. This technique involves applying a series of voltage pulses to the samples and measuring the resulting polarization response. The PUND measurements provide valuable information about the switching dynamics, remanent polarization, and coercive field of the materials. The results from the PUND measurements corroborate the findings from the hysteresis cycles, confirming the ferroelectric behavior of $La_{0.85}Er_{1.15}(MoO_4)_3$ and $LaEr(MoO_4)_3$ compositions.

To validate the measurements and provide reference points, well-known ferroelectric materials such as PZT and $BaTiO_3$ are included as ferroelectric references. Additionally, dielectric materials like Teflon and Al_2O_3 are selected as benchmarks for dielectric behavior. The comparison with these reference materials enhances the understanding of the measured data and validates the observed ferroelectric properties of $La_{0.85}Er_{1.15}(MoO_4)_3$ and $LaEr(MoO_4)_3$ compositions.

The results indicate clear ferroelectric behavior in $La_{0.85}Er_{1.15}(MoO_4)_3$ and $LaEr(MoO_4)_3$ compositions at room temperature, as evidenced by well-defined hysteresis loops and higher current

densities. These findings contribute to the understanding of ferroelectric materials and their potential applications in various technological fields.

This study is of great importance in the ability to differentiate when a hysteresis cycle can be misinterpreted as a ferroelectric response when it is actually due to dielectric losses. This distinction is crucial for accurate characterization of materials and avoids erroneous conclusions about their ferroelectric properties. By combining measurements of hysteresis cycles, current density, and the PUND method, an integrated approach is achieved that allows for a more precise differentiation between proper ferroelectric materials, improper ferroelectric materials, and dielectric materials.

Agradecimientos

En primer lugar, deseo agradecer a mi tutor, Manuel E. Torres, por su orientación, apoyo y conocimientos compartidos a lo largo de todo el proceso. Su experiencia y dedicación han sido invaluables para el desarrollo de este proyecto, y estoy muy agradecido por su guía y mentoría.

A mi familia y amigos, quiero expresar mi profundo agradecimiento por su constante apoyo y motivación. Han sido mi fuente de inspiración y han creído en mí desde el principio. Su confianza en mis capacidades han sido fundamentales para alcanzar este logro académico.

También quiero extender mi gratitud a aquellos que estuvieron a mi lado en momentos pasados y ya no lo están, pero cuyo impacto en mi vida y en este trabajo perdura. De igual manera, a aquellos que en un momento no estuvieron presentes en mi camino, pero que hoy en día forman parte de mi vida y han contribuido de manera significativa a mi desarrollo académico y personal.

Por último, pero no menos importante, deseo expresar mi gratitud a todas las personas que, de una forma u otra, han contribuido a la realización de este trabajo. Su colaboración, consejos y palabras de aliento han sido de mucho valor.

Contents

1. Introduction

En la introducción de este trabajo, se presenta una visión general de los molibdatos de tierras raras y sus aplicaciones en diversos campos. Se introduce el concepto de ferroelectricidad y se hace una distinción entre los materiales ferroeléctricos propios, los materiales ferroeléctricos impropios y los materiales dieléctricos. Los objetivos de este estudio son identificar correctamente el tipo de material al que pertenecen las muestras La-Er y evitar confusiones entre ciclos asociados a pérdidas dieléctricas y ciclos de histéresis. Además, se proporciona una breve reseña histórica sobre la ferroelectricidad y se destacan algunas de las aplicaciones importantes de estos materiales.

1.1 Concept

Oxide salts with rare-earth ions have become increasingly important in modern industry due to their high-tech uses. Amongst others, these compounds are relevant in solid-state lasers[2, 12], optical thermometers in sensors[22] and light-emitting diodes[19, 24, 28]. In particular, there is a specific type of these compounds which are further interesting due to their versatility, stability over time and temperatures, affordability and low toxicity[4, 11, 29, 30]. We are talking about molibdates of rare earths ($RE_2(MoO_4)_3$), where RE represents the rare earth element symbol. Also, these compounds can be easily modified in order to enhance certain luminescent characteristics.

Ferroelectric materials are substances which exhibit spontaneous reversible polarization in absence of an external electric field. The physical principle of this property is strongly related with crystal structure and the positioning of electric dipoles within the material.

In a ferroelectric material, the atoms (or molecules) which construct it are located in an ordered crystal structure. Each atom has a unique dipole moment due to the charge distribution of its structure. In normal conditions, these electric dipoles are randomly oriented and there is no net electric polarization in the material.

However, when an external electric field is applied to one of these materials, the electric dipoles align with its direction. This occurs since dipoles tend to align to minimize the systems' energy. As the fields' intensity rises, more dipoles align, increasing the net electric polarization.

The differentiating characteristic in ferroelectric materials is that they conserve the electric polarization even when the electric field is removed. The interaction between the dipoles and the crystal structure is what keeps the dipoles aligned. This property is called ferroelectric hysteresis.

In addition to classical ferroelectrics, there also exists materials which do not exhibit spontaneous polarization but they do enhance ferroelectric properties under certain circumstances. These are called improper ferroelectrics.

Improper ferroelectrics are characterized by their dependance of their crystal structure and the deformities induced by external factors like temperature, pressure, electric and magnetic fields. This phenomena can cause phase transitions in the material, which result in spontaneous electrical polarization.

In particular, temperature associated transitions are especially interesting. Above the critical temperature, the material finds itself in a low polarization or no-polar phase. However, when the temperature is below this value, it suffers a configuration change which results in a ferroelectric structure with spontaneous polarization.

It is important to make emphasis on the fact that improper ferroelectrics are highly dependant on external conditions, being much more sensitive to changes than conventional ferroelectrics. This makes them extremely interesting for multiple applications, such as nonvolatile storage, sensors and transductors.

1.2 Historical context

In the first quarter of the nineteenth century, piroelectricity was first observed by David Brewster in various crystals, including the well-known Rochelle's Salt[1]. In the final stages of that century, scientific duet Pierre and Paul-Jacques Curie demonstrated the piezoelectric effect[2] in the crystals that David Brewster had studied.

Later on, for military purposes quartz transducers (with a notable piezoelectric component) were used to develop ultrasonic submarine detection systems, building the basis for today's SONAR.

Analogously to the magnetic moment of atoms in magnetic materials, Debye developed in 1912 a theory around piezoelectricity phenomena by attributing electric dipole moment to certain type of molecules. With extreme coherence, he defined the electric counterpart of the Temperature of Curie (for paramagnetic cases), under which the material would exhibit polarization even in the absence of electric field. Later this year and as a result of continuing Debye's studies, Shrödinger introduced the term 'ferroelectric'.

Joseph Valasek is consider to be the scientist that demonstrated ferroelectricity, by exploring the relationship between the already known ferromagnetism with the dielectric properties of Rochelle's Salt. He established that this substance natural state was polarised, and presented the first sketch of a ferroelectric hysteresis cycle (1920)[27].

This was a turning point in the investigations in this field, making scientists wonder if the properties that Rochelle's Salt exhibited were also present in other materials.

In 1941, the first molecular theory of ferroelectricity was released, by John C. Slater. It was based on the idea that free hydrogen atoms were the reason for ferroelectricity.

With the second world war, investigation around this materials was again enhanced for submarine detection. In both USA and japan, $BaTiO_3$ was discovered and in 1945 it was demonstrated that this material was ferroelectric. This was in disagreement with the previous theory, since a compound without hydrogen showed ferroelectric properties. Based on this, in 1950 the Landau-Devonshire-Ginzberg (LDGT) theory was developed.

Materials with crystalline structure like the one $BaTiO_3$ displays are called perovskites and we can find in this group commonly used ferroelectrics: $SrBaTiO_3$ (BST) and $PbZrO_3$-$PbTiO_3$ (PZT). Nowadays, the use of lead is trying to be decreased.

Studies around improper ferroelectrics are more recent than those referred to classical ones. The concept of this new type of materials was born in the 1990s as non-ferroelectric materials were observed to exhibit ferroelectric properties in selective circumstances. Its study has involved many scientists and has improved constantly during recent decades.

Note that most references from this section have been extracted from A. Lükers' book[15].

1.3 Objectives

The ambition of this project is to develop robust criteria for classifying materials between ferroelectrics (proper and improper) and dielectrics. This topic is becoming increasingly important, since nowadays we do not possess anything like it. Many authors misinterpret graphs as hysteresis loops when in reality they are just looking at losses[9, 14, 16, 25, 31]. Not as often it happens the other way around, when actual hysteresis cycles are happening but they are interpreted as something else. To solve this, here we apply multiple techniques like current loops and PUND (Positive-Up-Negative-Down) analysis to distinguish between these cases. Results were compared with standard samples of pure ferroelectrics and dielectrics.

The hysteresis cycles will be studied to identify the polarization reversal and switching phenomena in proper ferroelectric materials. By examining the presence of distinct polarization states and analyzing the resulting hysteresis loops, the project aims to gain insights into the unique behavior of proper ferroelectrics. Improper ferroelectrics, on the other hand, will be investigated to explore their modified and lower magnitude polarization response, which may still exhibit similar but less pronounced hysteresis behavior. Dielectric materials, lacking permanent polarization, will serve as a reference for comparison, as they do not display hysteresis effects.

Furthermore, the density of current as a function of the applied electric field will be measured to investigate the conduction mechanisms and response of the different materials. This analysis will provide a deeper understanding of the electrical behavior and properties of each material type.

[1] $KNaC_4H_4O_6{\cdot}4H_2O$

[2] Generation of an electric charge in certain materials when subjected to mechanical stress or pressure. This effect highlights the conversion of mechanical energy into electrical energy and vice versa.

1.4 Motivation

The motivation for undertaking this project stems from articles like 'Ferroelectrics go bananas' [23] that discuss the issue of misinterpreting leakage current cycles as hysteresis loops in improper ferroelectrics. This realization prompted a deeper interest in investigating and understanding the complexities of characterizing ferroelectric materials accurately. The need to differentiate between different types of materials, specifically improper ferroelectrics, is of extreme relevance for nowadays industry. By employing a combination of measurement techniques such as hysteresis cycles, density of current analysis, and the PUND method, it becomes possible to discern with greater precision the nature of the samples under study.

Furthermore, another motivation lies in the quest to avoid ambiguities that can arise when analyzing experimental data. The presence of leakage currents or other external factors can lead to false interpretations of hysteresis cycles, potentially leading to incorrect conclusions about the ferroelectric behavior of a material. By carefully examining the subtle differences in electrical responses using various techniques, it becomes possible to untangle these complexities and ensure accurate characterization.

2. Synthesis of the Materials.

En el segundo capítulo, se abordan los fundamentos de la técnica de reacción en estado sólido y la síntesis, mediante esta técnica, de las soluciones sólidas $La_{2-x}Er_x(MoO_4)_3$ con x=0.85, 1, 1.15. Se describen las etapas clave del proceso, que incluyen la preparación de compuestos, la molienda y mezcla de los materiales, la compactación de las muestras, el tratamiento térmico y la colocación de electrodos. Se proporciona información sobre los equipos utilizados en cada etapa del proceso. Además, se destaca el uso de la difracción de rayos X como técnica para confirmar la obtención de los compuestos deseados y verificar su estructura cristalina.

2.1 Solid State Reaction.

The physics fundamentals behind solid state reaction method, also known as ceramic synthesis, are based in the chemical reaction that takes place in solid compounds at structural and molecular level. When the initial solid materials are subjected to thermal treatment, atom transfer between components takes place. The heat provides the energy to break existing bonds and form new ones.

The thermal treatment must imply reaching a high enough temperature to activate the reactivity of the materials, but below their fusion temperature. This way, atoms have enough energy to slide through the crystalline structure of the compounds, which is the whole purpose.

To ease this process where the reactants fuse into a sole product, we have to ensure that the molecules of both compounds are as close as possible to each other. This is achieved by integrating the reactants amongst each other with thorough mixing and pressing.

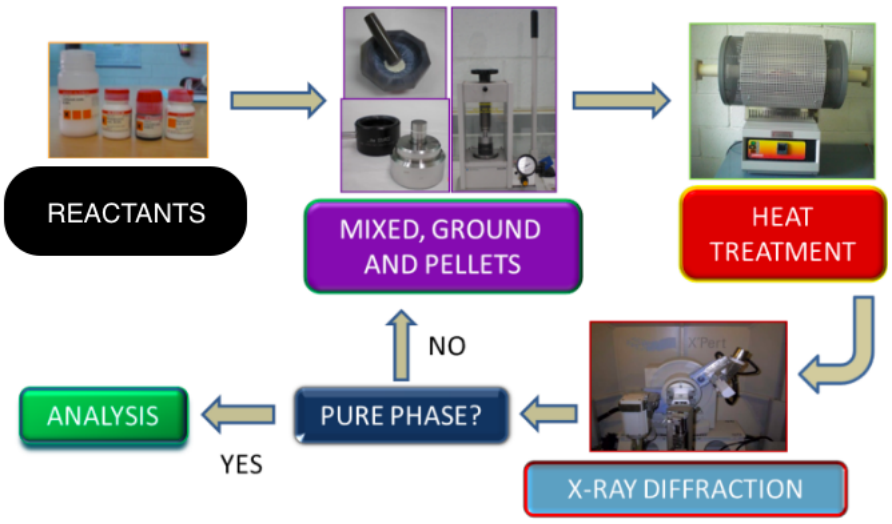

Figure 2.1: Outline of the steps in a typical synthesis of materials by solid sate reaction.

2.1.1 Preparation of initial compounds

To study the porperties of proper and improper ferroelectrics, different compositions of Lanthanum and Erbium molybdates were synthesised in order to continue previous studies from CCDD Research Group (ULL)[7].

The end product was three different proportions of $La_{2-x}Er_x(MoO_4)_3$ with x=0.85, 1, 1.15. However, in the lab we only have available the following initial compounds: La_2O_3, MoO_3 and Er_2O_3 (fig. 2.2). From these, we worked our way up to synthesize intermediate compounds ($La_2(MoO_4)_3$ and $Er_2(MoO_4)_3$) and eventually onto the final proportions. All the solid state reactions were carried out with the same procedures except some changes in the thermal treatments.

Figure 2.2: Starting reagents, from left to right: Erbium Oxide, Lanthanum oxide and Molybdenum Oxide

The first part of the procedure consists in defining the stoichiometric equations of the reactions:

$$La_2O_3 + 3MoO_3 \rightarrow La_2(MoO_4)_3$$

$$Er_2O_3 + 3MoO_3 \rightarrow Er_2(MoO_4)_3$$

$$(2\text{-}x)La_2(MoO_4)_3 + xEr_2(MoO_4)_3 \rightarrow 2La_{2-x}Er_x(MoO_4)_3$$

Now, the substances are to be weighed (fig. 2.3) appropriately and continue with the procedure. However, since the compounds have been resting at the lab for long periods of time, they could be hydrated with water molecules, meaning that a weight measurement could not to correspond to the actual quantity of the substance.

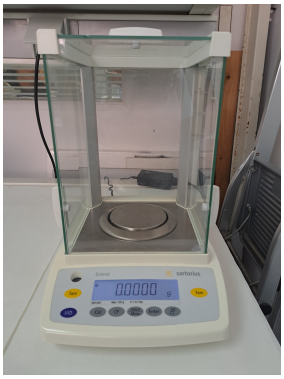

Figure 2.3: Precision balance employed to determine the mass needed from every compound for every solid state reaction.

To amend this, the initial reactants (La_2O_3, MoO_3 and Er_2O_3) were subject to a brief thermal treatment which we call precalcination, where we reach relatively low temperatures above the boiling point of water (fig. 2.4). This way, our compounds are not altered and we have evaporated the water that was prevailing.

The amount of substance that endured the precalcination process was calculated to be as of 10% more than what we would need for the solid state reaction to produce the desired outcome. See appendix for full details on the measurements that were taken.

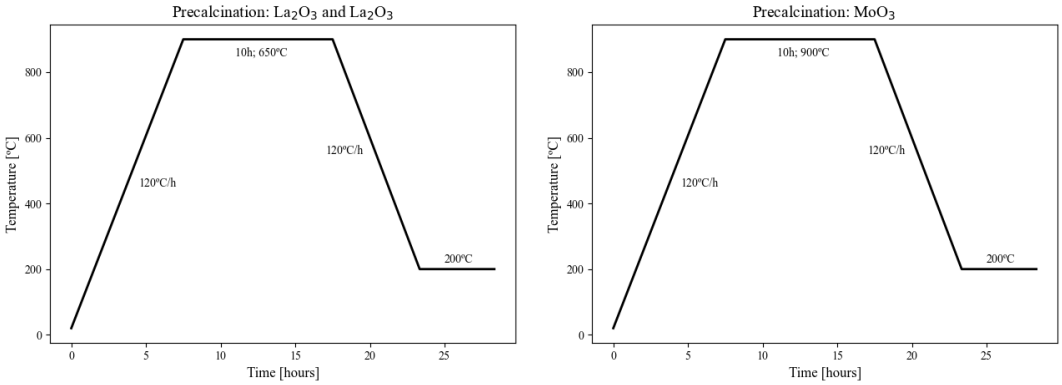

Figure 2.4: Precalcination processes for the starting reagents.

At this moment, we can assume that all the material we weigh is what its supposed to be, and we are ready to continue with the preparation.

2.1.1.1 Ovens and crucibles

It is interesting to take a moment to talk about the ovens (fig. 2.5) used both for the precalcination processes as well as the following thermal treatments. Carbolite laboratory ovens are designed with a specific configuration, where the primary heating element in is the resistor, which generates heat when electrical current passes through it. These resistors are strategically placed around the tube to ensure even and uniform heat distribution throughout the sample. The tube acts as a chamber or enclosure that holds the sample to be heated.

These ovens incorporate a temperature control system that enable us to set and maintain specific temperature levels.

The design of the ovens promote efficient heat transfer, allowing for rapid and uniform heating of the sample. The placement of resistors around the tube ensures that the entire sample is exposed to heat, minimizing temperature gradients and providing reliable results.

However, even though its minimized, there is a temperature gradient between the resistors temperature and the sample's temperature. This is not a huge problem, since it is a systematic feature which in our case has been tabulated and can be accounted for.

Figure 2.5: Ovens used for the materials' synthesis.

For the precalcination, the samples are in powder form, in order to favour the escape of water molecules (with a high surface area to volume ratio). To easily manage the whole sample and as to not lose substance, the material is placed in platinum crucibles for its heating.

Platinum crucibles are highly regarded in laboratory settings for their exceptional properties that make them ideal for heating materials in thermal treatments. Platinum has an extremely high melting point of around 1,768ºC[17], this allows platinum crucibles to withstand and maintain their structural integrity under intense heat, making them suitable for a wide range of thermal treatments. Furthermore, platinum exhibits excellent thermal conductivity, meaning it efficiently

transfers heat to the sample within the crucible, ensuring that the heat is evenly distributed throughout the material

More importantly, this element is chemically inert. It is highly resistant to corrosion and does not react with most chemicals, making it suitable for a broad range of materials. Also, platinum has low reactivity with various elements including oxygen, nitrogen, and carbon. This characteristic prevents unwanted reactions or contamination of the sample during thermal treatments, ensuring accurate and reliable results.

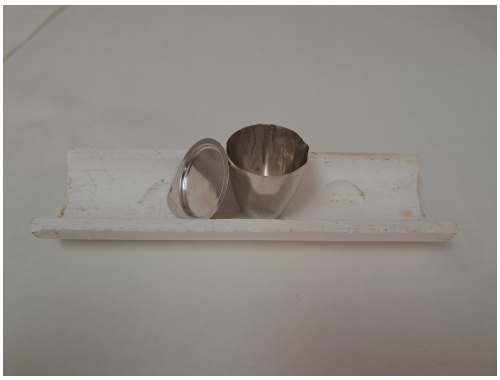

Figure 2.6: Platinum crucible where samples are located to be heated inside the oven.

2.1.2 Grinding and mixing

Once we have the correct amounts, we must take some actions in order to favour the different molecules to interact with each other. Our reactions are of the form A + B $\rightarrow$ C. The solid state reactions consists of blending grain A with B to form a homogeneous grain C.

When compound C is formed from reactants A and B, it creates a situation where the ions of A and B need to diffuse through the interface between the reactants and the compound. This process is known as counter-diffusion.

As the reaction progresses, the concentration gradient of the ions A and B across the interface increases. This means that there is a higher concentration of A and B on one side of the interface compared to the other. Due to this concentration gradient, the ions have to travel a longer distance to reach the other side of the interface, resulting in slower diffusion rates.

The counter-diffusion of ions A and B becomes more pronounced as the reaction continues. This is because the formation of compound C consumes A and B, leading to a decrease in their concentrations near the interface. As a result, the concentration gradient across the interface becomes steeper, exacerbating the counter-diffusion problem.

The consequence of this counter-diffusion is a decrease in the overall reaction rate. As the ions A and B have to travel a longer distance through the interface, it takes more time for them to react and form compound C.

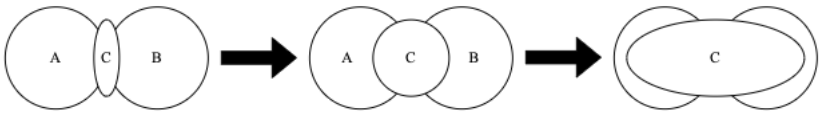

Figure 2.7: Representation of solid state reaction. As the reaction develops, the concentrations of grains A and B decrease in favour of the concentration of grain C (the product).

We start this process by grinding the reactants together during one hour for the first reactions and two hours for the final one, using a mortar (fig. 2.8).

We have chosen to use a mortar fabricated from agate, a form of crystalline quartz. Agate is a hard material, resistant to the natural wear, which makes it ideal for blending ceramic compounds[1]. Furthermore, agate has very low porosity, minimizing cross contamination between different samples and helping to maintain the purity of the reactants.

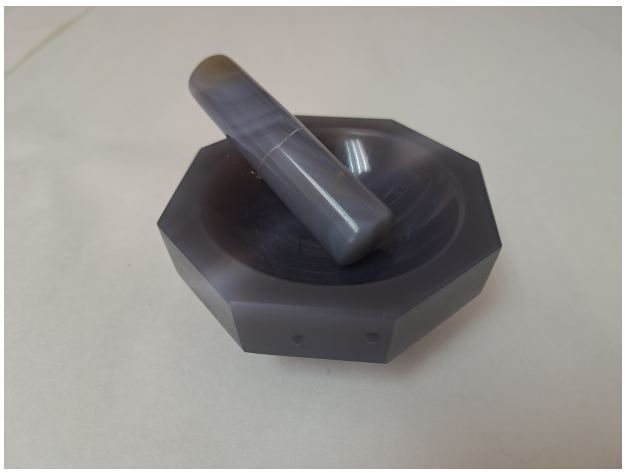

Figure 2.8: Agate mortar used for all of the grindings carried out.

The process itself implies crushing and grinding the reactants in dust form using manual pressure. As we apply this pressure, we must crush in circular motion in both directions. The compounds are subjected to compressing and cutting forces, easing the fragmentation of particles and intimate mixing.

Other important factors to take in mind during this step include carefully cleaning the mortar (to avoid previous contamination) and taking enough time until the mixture is visibly homogeneous.

2.1.3 Compacting

Compressing the initial powder materials into pellets before the thermal treatment is an essential step. This process involves subjecting the loose powder materials to high pressure with a hydraulic press (fig. 2.9(a)) to create compacted forms with enhanced density and structural integrity. The compression of the powder materials offers several advantages and plays a crucial role in the subsequent characterization and analysis of the materials.

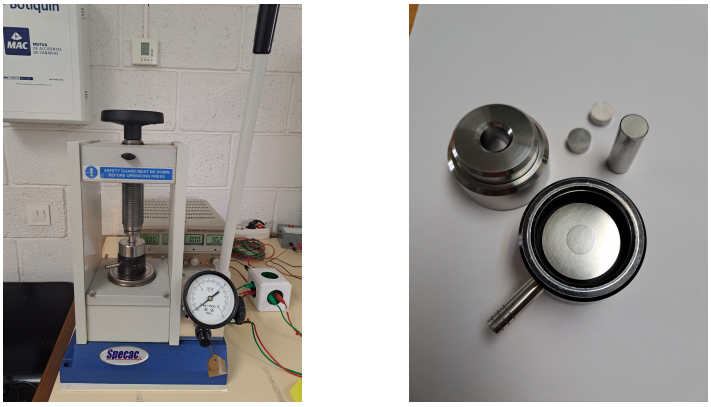

(a) (b)

Figure 2.9: a) Hydraulic press with handle, with which manual force is applied gradually until the desired pressure is achieved. b) Mold where the powder to be compressed is located.

To obtained the desired profile of pellets, a mold (fig. 2.9(b)) is used, ensuring a constant diameter of the pellet as well as uniform faces. The powder is located inside the hollow cylinder and, with the aid of a piston, the sample is compressed by the hydraulic press to a pressure of three tons. This final pressure was agreed upon previous experiences where 29,420Pa/m^2 (3 tons) showed the best results. One could think adding extra force would always be favourable for the pellets integrity, however, above three tons, the pellets have shown to become too brittle and fragile, even though the atoms could be closer together. This pressure provides a compensation between proximity of atoms and assured structural integrity. Notice the cylindrical feature in the (black) base of the mold, this is hollow and connected to the inner section to carry the function

of providing an escape for the air compressed. If this did not exist, the powder the pellets would have air pockets inside, weakening its structure.

Porosity is another matter to take into account that is explained in section 2.1.5.

One of the primary benefits of compressing the powder materials is the improvement in density. By applying pressure, the particles are forced to come into closer contact with each other, reducing the empty spaces between them. This results in a higher density of the material, which can have a significant impact on its physical and electrical properties.

Furthermore, the compression process promotes better mixing and homogeneity of the powder materials. As the particles are compressed, they are forced to interact more closely, facilitating the mixing of different components. This ensures a consistent composition throughout the sample, which is essential for obtaining accurate and reproducible results in subsequent analyses.

Compressing the powder materials also contributes to the structural integrity of the samples. Strong interparticle bonds are formed, enhancing the mechanical strength and stability of the material. This is especially important when the samples are subjected to subsequent high temperature thermal treatments.

Moreover, the compressed form allows for consistent heat transfer during thermal treatments. The uniform shape and size of the pellets enable uniform distribution of heat, ensuring that all parts of the sample experience similar thermal conditions. This promotes uniformity in the structural and chemical transformations that occur during the thermal treatment, resulting in more reliable and reproducible material properties.

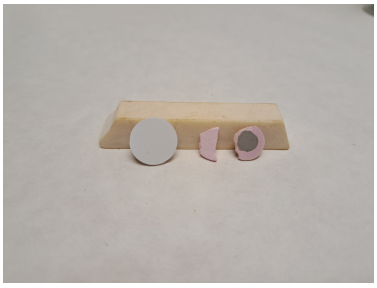

Figure 2.10: Examples of the different pellets obtained with solid state reaction. From left to right: $La_2(MoO_4)_3$, $Er_2(MoO_4)_3$ and $LaEr(MoO_4)_3$ with platinum paint electrodes already fixed.

2.1.4 Thermal treatment

Following the preparation of the initial compounds, the subsequent grinding and mixing, and the compaction into pellets, the thermal treatment plays a vital role in achieving the desired crystal structure and properties of these materials.

Thermal treatment, also known as heat treatment or calcination, involves subjecting the compacted samples to controlled temperature conditions for a specific duration. This process induces various chemical and physical transformations within the material, leading to the formation of the desired crystalline phases. The thermal treatment is carried out in a controlled environment, alike the the mentioned precalcination.

The specific temperature and duration of the thermal treatment are carefully determined based on the desired phase transformation and the properties required for the target materials. For $La_2(MoO_4)_3$ and $Er_2(MoO_4)_3$, these parameters were determined through prior research and experimentation.

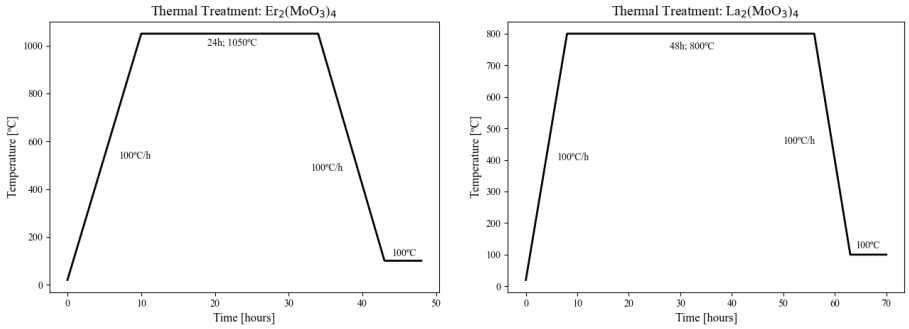

Figure 2.11: Thermal treatment for $La_2(MoO_4)_3$ and $Er_2(MoO_4)_3$

As for the final compounds, a similar process was followed (fig. 2.12), with the same temperature for all three proportions but different dwell times. Again, the nature of the thermal treatments were based of previous successful experiments with similar compounds. The main change between this treatments and those of figure 2.11 is the final stage. Now, we subject the samples to a quick-cooling period which we call quenching. Quenching cooling is performed to "freeze" the material's microstructure at a specific phase or state, preserving the desired properties obtained during the thermal treatment. It helps prevent the formation of undesired phases or structures that may occur during slow cooling processes.

Ideally, the sample would endure an instant change of temperature from 900ºC to room temperature. However, immediate temperature changes are not possible in reality. They can be approximated using cooling liquids like oil or water but in our case this could compromise the samples integrity and contaminate it. Fuerthermore, the oven itself does not have the ability to cool its content, complicating even more the quenching stage. The most that we could approximate to the ideal case was by, once the moment arrived, turning off the resistances of the ovens. This is far from ideal but in some way, it at least provided a stable cooling environment; preventing other phases from being created.

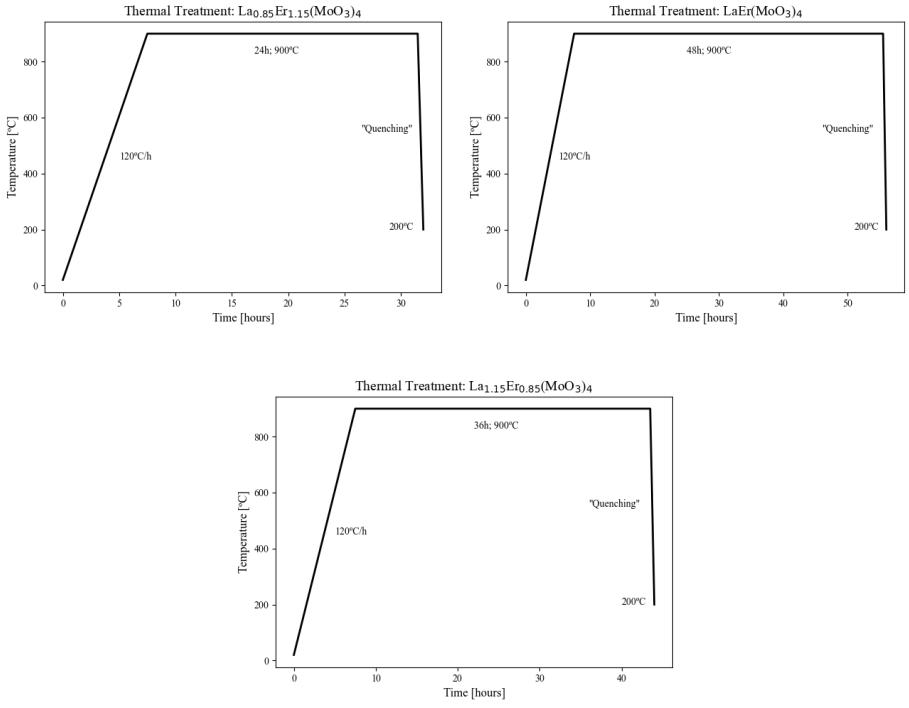

Figure 2.12: Thermal treatment for $La_{2-x}Er_x(MoO_4)_3$, x=0.85, 1, 1.15.

2.1.5 Fixing the electrodes

After the synthesis of the samples and their formation into pellets through the process of compaction, the next step involves fixing electrodes onto the samples. This step is crucial as it enables the electrical measurements to take place with our equipment (more on it later).

To fix the electrodes, platinum paint is used. Platinum is chosen due to its excellent electrical conductivity, stability, and compatibility with high-temperature processes, as mentioned earlier. The paint is carefully applied to the surfaces of the sample where the electrodes are desired (fig. 2.10).

Once the platinum paint has been applied, the samples are subjected to a drying process. This involves placing the samples in an oven and gradually increasing the temperature up to 750°C. The elevated temperature allows the paint to cure and adhere firmly to the surface of the samples. After the drying process, the samples are rapidly cooled, or quenched, to room temperature to complete the fixation of the platinum electrodes.

Compacting and fixing the electrodes are crucial stages in avoiding porosity in the sample. The presence of porosity can introduce several problems in ferroelecric measurements, affecting the accuracy and reliability of the results. For example, porous materials may have regions or voids within their structure that cannot be fully polarized. As a result, the measured hysteresis loops may not reflect the complete polarization behavior of the material. This incomplete polarization can lead to distorted or altered hysteresis curves, making it challenging to accurately analyze the material's ferroelectric properties.

Furthermore, porosity can significantly reduce the remanent polarization of the material. When it is present, the effective polarization of the sample decreases, resulting in smaller or less prominent hysteresis loops.

Higher levels of leakage current could also be exhibited compared to dense samples. The presence of pores provides additional paths for the leakage of electric charge, leading to increased current flow. This increased leakage current can contribute to elevated background noise and affect the measurement accuracy, making it challenging to distinguish the true ferroelectric response.

2.2 X-Ray Diffraction

As a wave approaches an obstacle with dimensions close to its wavelength, it gets diffracted. X-rays wavelength range from 10pm to 10nm in the electromagnetic spectrum. In crystalline structures, the inter-atomic distance is approximately 1Å. Hence, X-rays around 1Å are used to study this type of materials. A monochromatic ray of this radiation is shone into the sample at different angles and the different intensities of the diffracted rays are received by a detector. Bragg's Law (equation 2.1) allows us to analyse the results and obtain conclusions, since when this condition is satisfied, it means rays diffracted by the parallel planes of the crystal structure interfere constructively.

$$2\lambda = 2d \cdot sin(\theta) \tag{2.1}$$

Where n = whole number, λ = wavelength, d = distance between crystal planes, θ = angle of incidence.

The resulting pattern is unique for each crystalline structure, making it an excellent technique for assuring the material synthesised is the desired outcome.

In our case, samples were sent to *Universidad de La Laguna* facility SEGAI (*Servicio General de Apoyo a la Investigación*). A PANalytical Empyrean diffractometer was used with Cu-K_α wavelength, corresponding to two lines (λ(Cu-K_α1) = 1.54056Å and λ(Cu-K_α2) = 1.54443Å), passing through a Ni filter, a fixed divergence slit of $1/2^o$, and a receiving slit of $1/8^o$. The measurements were taken in an angular range of $5° < 2\theta < 80°$ with a step size of 0.02^o and a time of 57s. The software used for identification and refinement were the Inorganic Crystal Structure Database (ICSD)[10] and the FullProf program package[21].

The results obtained the samples can be observed in figures 2.13 and 2.14. They were successful in obtaining the desired phases: α for $La_2(MoO_4)_3$, γ hydrated for $La_2(MoO_4)_3$ and β' for $La_{2-x}Er_x(MoO_4)_3$.

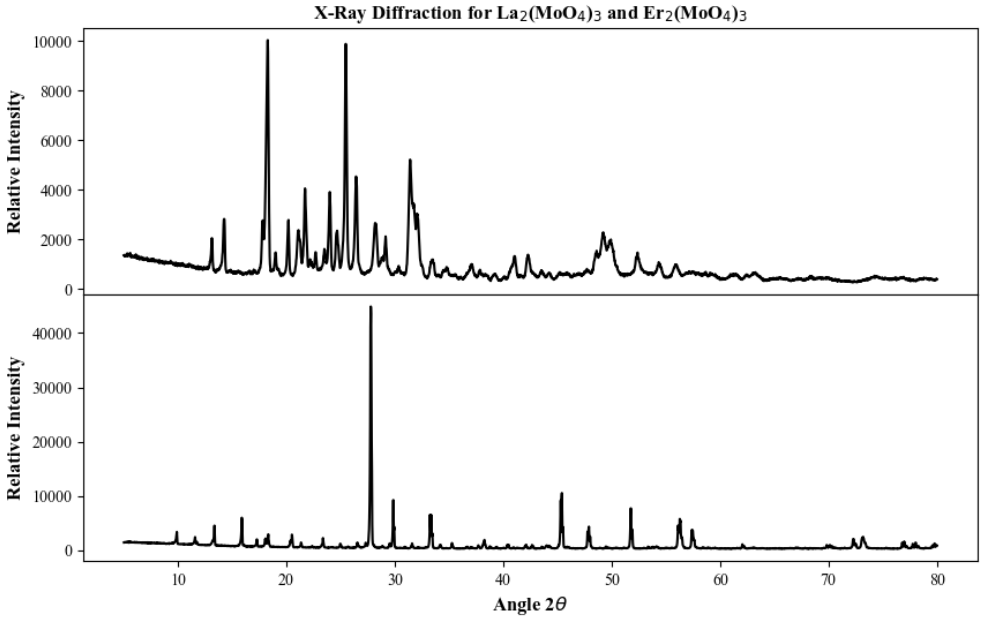

Figure 2.13: From top to bottom: $Er_2(MoO_4)_3$, $La_2(MoO_4)_3$.

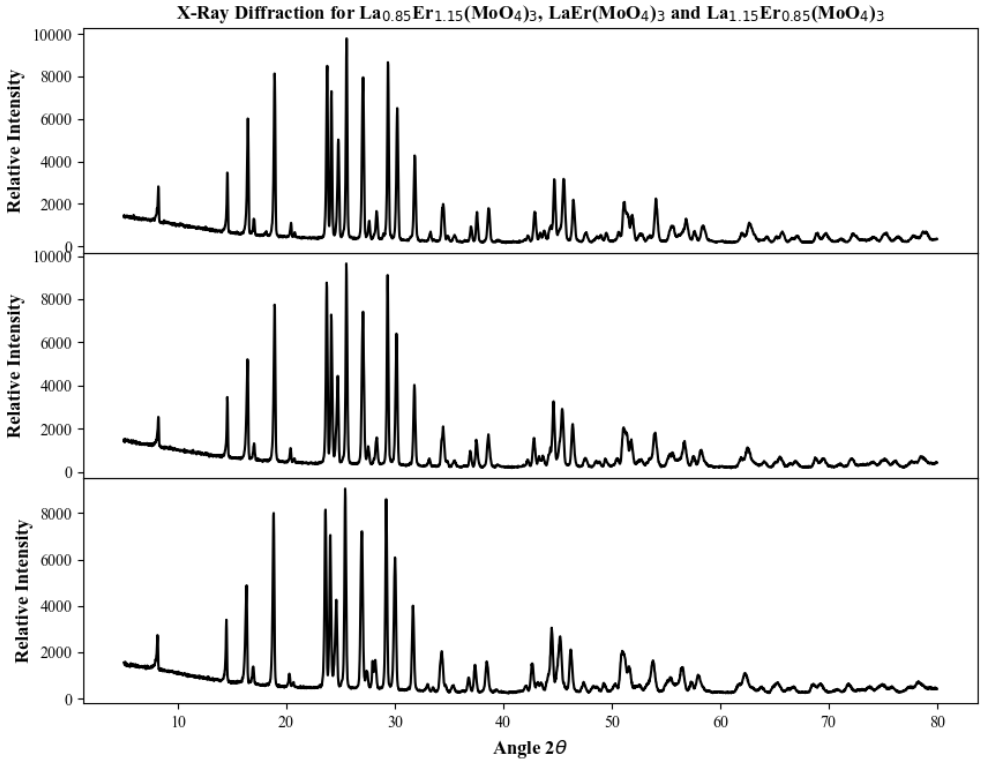

Figure 2.14: From top to bottom: $La_{0.85}Er_{1.15}(MoO_4)_3$, $LaEr(MoO_4)_3$ and $La_{1.15}Er_{0.85}(MoO_4)_3$. Notice how the features slightly shift to the left as the Lanthanum concentration increases. Also, appreciate how the final profiles are a combination of both seen in figure 2.13.

3. Experimental method

A continuación, se detalla el equipo utilizado, el sistema Radiant, para realizar los ensayos de histéresis, densidad de corriente y el método PUND en la solución sólida $La_{2-x}Er_x(MoO4)3$ con x=0.85, 1 y 1.15). Además, se mencionan los materiales de referencia utilizados, como el PZT y el $BaTiO_3$ para las mediciones de ferroeléctricos, y el Teflon y el Al_2O_3 para las mediciones de paraeléctricos. Se describe cómo se llevan a cabo las medidas, destacando el uso del método de tierra virtual en lugar del circuito clásico de Sawyer-Tower para los ensayos de histéresis. También se mencionan las técnicas de espectroscopía de impedancia y calorimetría diferencial de barrido (DSC) habitualmente utilizadas para determinar las temperaturas de transición de fase en las muestras.

3.1 Radiant Systems equipment

For the measurements, hardware and software from Radiant Systems[20] was used. This manufacturer is highly regarded in this field of study and is specialized in measurements and analysis of electrical properties of materials.

Figure 3.1: Radiant Systems hardware used for Hysteresis, Current Density and PUND measurements.

The Radiant equipment includes an auxiliary high voltage source of 10kV, which allows to apply a controlled electrical field to the samples. The software (Vision), developed by Radiant Systems is a complementary tool which contributes with an easy interface to control the equipment, acquire data and perform analysis.

As for the sample, it is positioned inside a chamber(fig. 3.2(a)), which Radiant Systems call High Voltage Test Fixture (HVTF). It is an essential component of the measurement setup used in materials characterization, providing a controlled environment for the samples during electrical measurements and ensures proper electrical connection to the Radiant system.

The chamber is designed to provide electrical insulation and protection to prevent any external interference or electrical leakage. It is made of high-quality insulating material that can withstand high voltages without breakdown or degrading.

Inside the chamber, the sample is securely positioned and aligned with the electrodes attached to it. These electrodes are connected to the Radiant system, which applies the desired electrical

signals and measures the corresponding response. The connection between the electrodes and the Radiant system is established using high-voltage cables that can handle the required voltage levels.

It also guarantees a controlled environment around the sample. This includes factors such as temperature, humidity, and atmospheric conditions to ensure accurate and repeatable measurements.

Nevertheless, some times the high voltages can cause the air surrounding the sample to ionize, something we call the dielectric rupture of the air. This causes chaotic measurement. To prevent this situation, we try to minimize the air packed inside the chamber by adding silicone to the surrounding areas of the sample (fig. 3.2(b)).

(a) (b)

Figure 3.2: High Voltage Test Fixture: Teflon sample holder.

Hysteresis cycles measurements were carried out, looking to study the change in polarization in response to external and variable electric field. Furthermore, current density was plotted against voltage; supplying information about the conductivity of the samples. Finally PUND (Positive-Up-Negative-Down) method was also used. This procedure consists in applying positive and negative electric field pulses and measuring the corresponding response. These are related to the commutation properties and the stability of the materials.

3.1.1 Reference Materials

This study relies importantly in comparing our results with reference samples, for which we understand their behavior and properties in most conditions. In the following, a brief introduction is given about these reference materials.

3.1.1.1 Ferroelectrics

- PZT: Lead zirconate titanate; $Pb(Zr_xTi_{1-x})O_3$ $(0 < x < 1)$. It is a ceramic perovskite material that shows a marked piezoelectric effect. It is used in a number of practical applications such as ultrasonic transducers and piezoelectric resonators. It is a white to off-white solid.[13]

- $BaTiO_3$: Barium titanate (BTO) is an inorganic compound with chemical formula BaTiO3. Barium titanate appears white as a powder and is transparent when prepared as large crystals. It is a ferroelectric, pyroelectric, and piezoelectric ceramic material that exhibits the photorefractive effect. It is used in capacitors, electromechanical transducers and nonlinear optics.[5]

3.1.1.2 Dielectrics

- Teflon: synthetic fluoropolymer made up of tetrafluoroethylene $[C_2F_4]$ monomer. It is non-reactive and a proper insulator.[18]

- Al_2O_3: Aluminium oxide, commonly called alumina is an electrical insulator but has a relatively high thermal conductivity for a ceramic material. Aluminium oxide is insoluble in water.[3]

3.1.2 Hysteresis

As explained earlier, the physical reason behind hysteresis cycles are the existence of domains and the inversion of polarization. A domain is a region of the material with uniform polarization, and the hysteresis cycles take place due to the reorientation of these domains in response to changes in the electric field applied.

In a proper ferroelectric, this change in the sign of the polarization is not instantaneous. Instead of changing abruptly from a polarised state to another one, domains experiment a gradual transition as the magnitude of the electric field rises. As a result, we obtain a gentle increase of the polarization, known as ascending hysteresis loop. When the direction of the, the domains can maintain their previous orientation due to the presence of energetic barriers. This implies that polarization does not revert immediately and can require a more powerful inverse electric field for the domains to reorientate in the opposite direction. In similar fashion, this causes a gentle decrease of the polarization, known as descending hysteresis loop. In this type of materials, the profiles of these cycles tend to be symmetric, meaning the ascending and descending cycles mostly superpose each other. Also, the size and shape of the cycle are strongly related to the intrinsec properties of the material, such as its coercitivity, which is the instensity of the electric field required to invert the polarization.

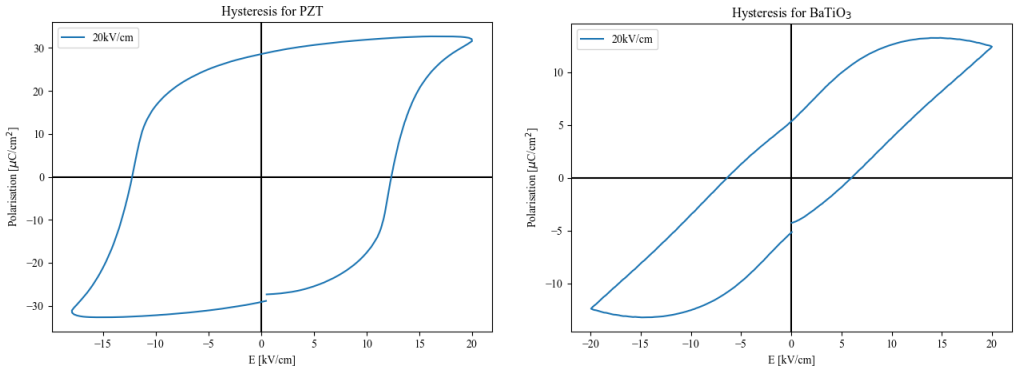

Figure 3.3: Hysteresis loops for the reference ferroelectrics: PZT and $BaTiO_3$. Notice a clear saturation of the polarization. More ferroelectric materials tend to exhibit this saturation sooner than those less ferroelectric.

In contrast, improper ferroelectrics do not exhibit as pronounced hysteresis loops and not always, only under specific circumstances.

Dielectric materials do not present permanent polarization, which is reflected in their hysteresis profiles. The relation of polarization against electric field is lineal and directly proportional. As electric field increases, polarization rises proportionately without experiencing any type of inversion or significant change in the direction of polarization. Graphically, the hysteresis cycle of a dielectric is represented as a straight line which crosses the origin; there is no loop formation or abrupt changes in the polarization. They have a linear and predictable response. However, sometimes these materials do exhibit a cycle that is related to losses and can be misinterpreted (fig. 3.4(B)), making hysteresis measurements insufficient on their own when characterizing certain materials.

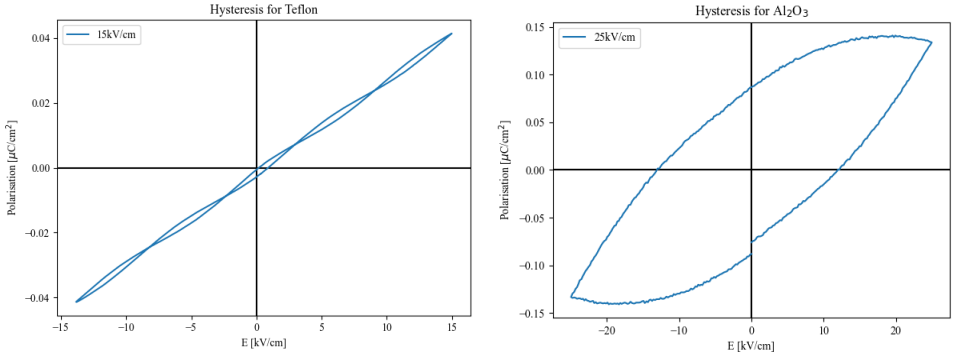

(a) (b)

Figure 3.4: Hysteresis loops for the reference paraelectrics: Teflon and Al_2O_3. Clear linear behavior is observed in (a). (b) exhibits a more cyclical curve, however this is not due to ferroelectricty, as will be later explained.

The hysteresis routine of Radiant Systems uses a method called 'virtual ground' with a triangular signal instead of the classical circuit Sawyer-Tower with a sine wave.

The Sawyer-Tower method utilizes a voltage divider comprising a capacitor for measurement and a reference capacitor. The voltage produced across the reference capacitor is directly related to the charge stored within the capacitor of interest. However, this method can have several issues which lead to inaccurate measurements that are greater than the order of magnitude associated with the electric phenomena of improper ferroelectrics.

One of the main issues is the leakage current of the reference capacitor. Over time, the reference capacitor may exhibit a small amount of current leakage, which can impact the accuracy of the voltage measurement. This leakage current can result in an additional voltage drop across the reference capacitor, leading to errors in the measured voltage across the ferroelectric capacitor.

Another undesirable effect is the parasitic capacitance associated with the reference capacitor. The presence of parasitic capacitance can introduce additional capacitance in parallel with the ferroelectric capacitor, altering its effective capacitance value. This can lead to inaccuracies in the measurement of the ferroelectric capacitors' charge or voltage, affecting the overall precision of the system.

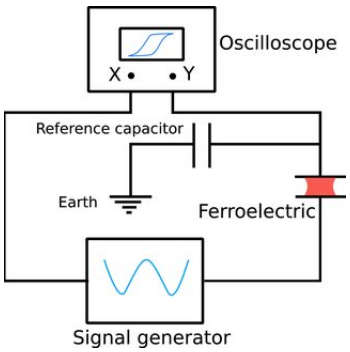

Figure 3.5: Sawyer-Tower circuit configuration[6].

On the other hand, the virtual-ground method measures the charge stored in the ferroelectric capacitor by integrating the current required to maintain one terminal of the sample at 0V, hence the name virtual ground. With no reference capacitor, we drastically reduce the unwanted effects earlier mentioned.

Triangular pulses are performed on the sample, going through the sequence 0V - V_{max} - 0V - (-V_{max}) - 0V.

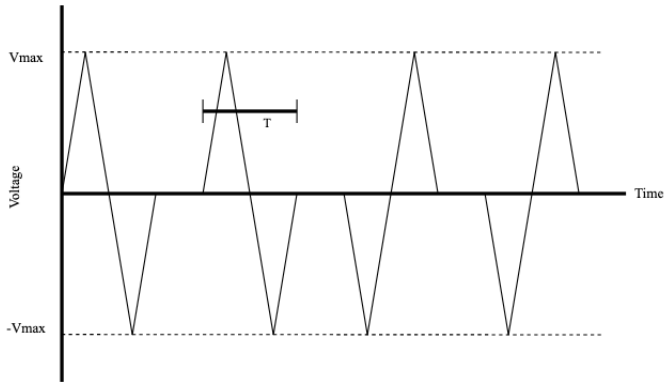

Figure 3.6: Representation of the triangular signal samples are subjected to in the hysteresis routine. T = Period.

3.1.3 Current Density

This concept was first introduced the french physicist André-Marie Ampère in the nineteenth century. Ampère developed the mathematical theory of electrodynamics, establishing the basis for the comprehension of electromagnetic phenomena. His work was vital for the development of fundamental laws like Ampère's Law, relating electric current with magnetic field.

The current density (J) is a fundamental concept in electromagnetism and represents the amount of current flowing through a given area. It is defined mathematically as the ratio of the current (I) passing through a conductor to the cross-sectional area (A) perpendicular to the current flow.

Mathematically, the formula for current density is:

$$J = \frac{I}{A} \tag{3.1}$$

Where J is the current density(A/m^2), I is the current(A) and A is the cross-sectional area(m^2).

More interestingly, J can be associated with the materials conductivity (σ):

$$J = \sigma \cdot E \tag{3.2}$$

Where σ is the conductivity of the material (S/m), E is the electric field (V/m).

This equation highlights the direct proportionality between the electric field and the current density, with the material's conductivity acting as a proportionality constant.

However, the relationship between current density and electric field can be more complex in certain materials, as they may exhibit nonlinear or frequency-dependent behavior.

Knowing the current density is essential to understand the electrical behaviour of ferroelectric materials in a wide range of technological applications such as information storage, piezoelectric transducers, high-capacity condensers and sensor; amongst others.

In our measurements, we will be plotting current against electric field. Qualitatively this is equivalent to plotting current density, since they are directly proportional, only dependant of the area of the electrodes (equation 3.1).

In proper ferroelectrics, is common to observe the presence of two spikes in the current density against voltage curve. These are associated with the change in polarity of the sample when the electric field applied is inverted. The first spike corresponds to the initial polarization of the material meanwhile the second one indicates its inversion.

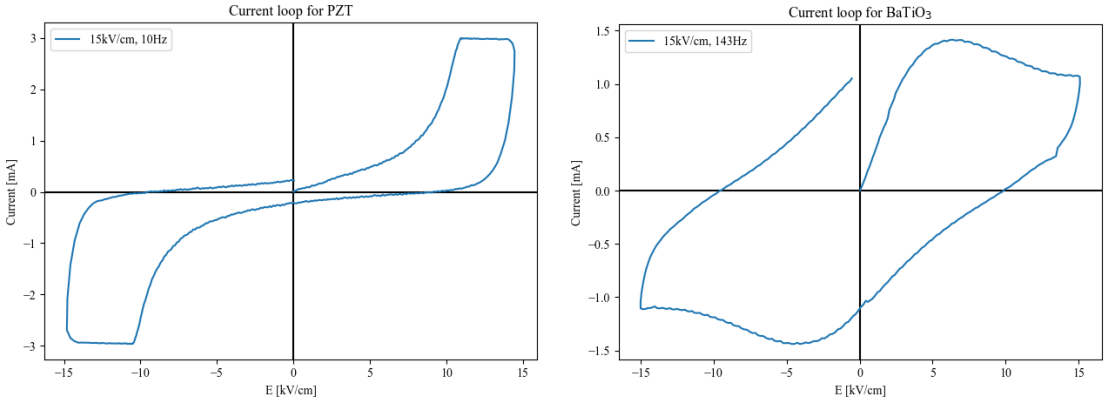

Figure 3.7: Hysteresis loops for the reference ferroelectrics: PZT and $BaTiO_3$.

In improper ferroelectrics, we can observe a similar pattern, but with a significantly lower amplitude in comparison with the typical forroelectric amplitude. Logically, this happens to their weaker polarization behaviour, causing also much smaller spikes.

In paraelectrics, the absence of a ferroelectric phase transition means that there is no hysteresis or polarization reversal as the electric field is varied. As a result, the concept of current loops, which is based on the switching of polarization directions, is not observed in paraelectric materials.

Instead, in these materials, the response to an applied electric field is characterized by a linear relationship between the electric field and the induced polarization. This linear behavior is governed by the material's dielectric constant and its ability to store and release electrical energy.

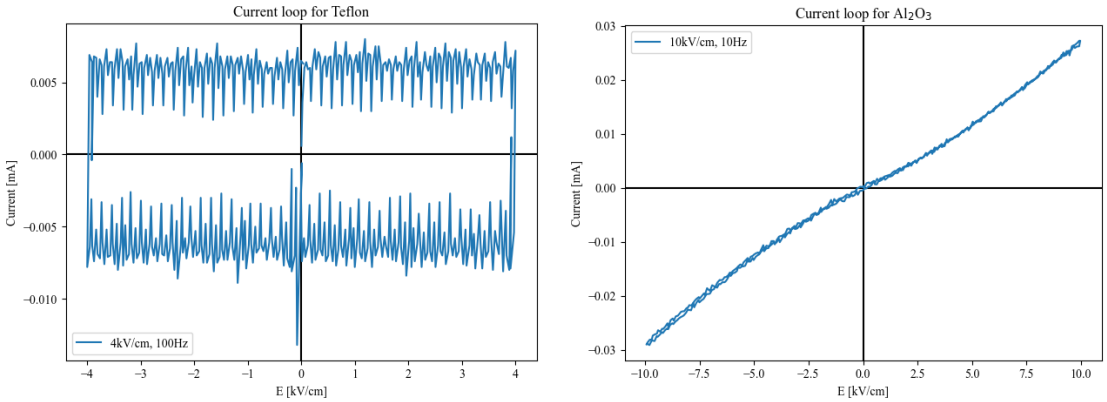

Figure 3.8: Current loops for the reference paraelectrics: Teflon and Al_2O_3.

3.1.4 PUND method

PUND (Positive-Up-Negative-Down) method is a not so common technique used in the study of ferroelectric materials. It consists in performing a sequence of five pulses which allow to obtain precise information about the behaviour of the sample (fig. 3.9). The purpose of the first pulse is to establish the initial polarization state of the sample, in the opposite direction of the maximum voltage (V_{max}). Here, no measurements take place, it is just about fixing the polarization.

The second pulse inverts the polarization of the material and we register the difference between the initial and the current polarization. This measurement indicates the commutation capacity of the material. Immediately after, we make the voltage 0, in order to guarantee precise measurements of the remanent polarization and other parameters.

Once the sample has 'relaxed', a second measurement is done at 0V. Consequently, we obtain information about the polarization that has not been inverted. The third pulse is a clone of the second one, with the same measurements, but in this case the remanent polarization of the sample does not commute, meaning the measurement represents the non-remanent contribution.

The fourth and fifth pulses are replicates of the previous two, but in the opposite sign of the electric field.

The relaxation time of electric dipoles plays a crucial role in accurately measuring the remanent polarization of ferroelectric materials. When an external electric field is applied to a ferroelectric material, the electric dipoles within the material align themselves with the field. Once the field is removed, the dipoles do not instantaneously return to their original random orientation. Instead, they undergo a relaxation process, transitioning back to their equilibrium positions over a certain period of time.

The relaxation time refers to the characteristic time it takes for the dipoles to relax and reach their equilibrium positions. This time can vary depending on several factors, including the material composition, temperature, and the presence of impurities or defects. The relaxation time is typically on the order of microseconds to milliseconds in ferroelectric materials.

If the relaxation time is relatively short compared to the measurement time scale, the remanent polarization will accurately reflect the true polarization state of the material. However, if the relaxation time is long, the remanent polarization may not fully represent the actual polarization due to incomplete relaxation.

That is why it is important to adequately select the time between pulses when carrying out the PUND method.

Pulse	Applied Voltage	Measurement
1	$-V_{max}$	-
2	V_{max}	P^*
-	0	P^*_r
3	V_{max}	P^h
-	0	P^h_r
4	$-V_{max}$	$-P^*$
-	0	$-P^*_r$
5	$-V_{max}$	$-P^h$
-	0	$-P^h_r$

Table 3.1: In total, 8 parameters are measured with the PUND method. This table shows when they are measured in relation to the five pulses with amplitude V_{max} and relaxation time of 1s.

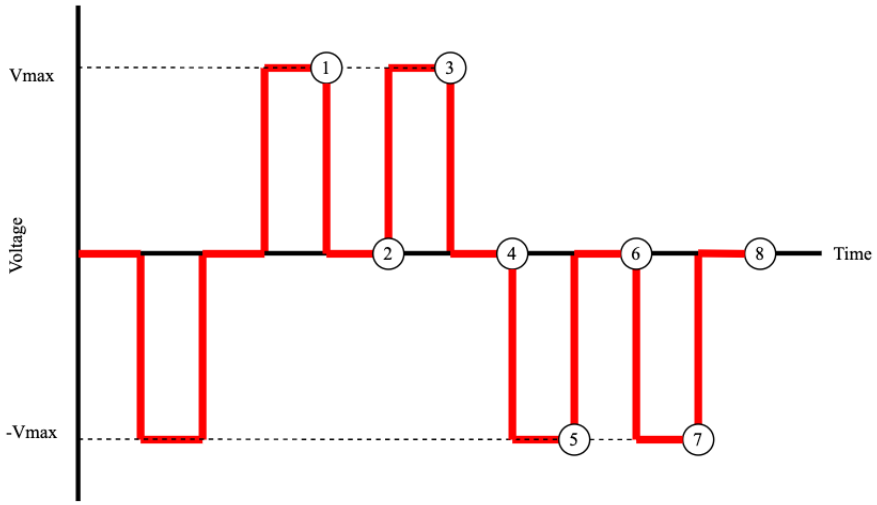

Figure 3.9: Graph of voltage against time which represents when the 8 parameters related to remanent polarization are measured. Legend: 1=P^*, 2=P^*_r, 3=P^h, 4=P^h_r, 5=$-P^*$, 6=$-P^*_r$, 7=$-P^h$, 8=$-P^h_r$

The measurements taken can be more easily visualized in figure 3.10. With this methods based on pulses and relaxation times, we obtain precise measurements of the parameters. Even though we do not obtain the full profile of the hysteresis loop, we can deduce the properties of the materials and consequently if they are under a ferroelectric or paraelectric regime.

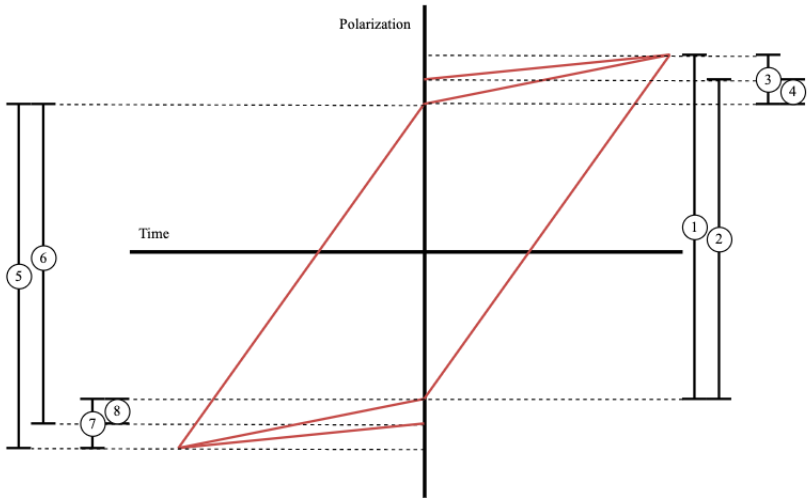

Figure 3.10: Same 8 parameters represented again. This time their actual polarization value. They sketch out a hysteresis loop.1=P^*, 2=P_r^*, 3=P^h, 4=P_r^h, 5=-P^*, 6=-P_r^*, 7=-P^h, 8=-P_r^h

3.2 Phase Transitions

The justification of this study highly depends on the fact that ferroelectric materials present a phase transition at certain temperatures, going from ferroelectric regime to paraelectric as temperature increases.

When the temperature rises, the mobility of the electric domains also increases. Essentially, this causes the domains to be more responsive to changes in external fields applied. Hence, remanent polarization decreases with temperature. Ultimately, this means that hysteresis cycles begin to fade away and become more alike to the ones displayed by dielectric materials like Teflon.

The transitions can be detected by several methods. At Universidad de La Laguna, there are two main procedures: impedance espetroscopy and DSC (Differential Scanning Calorimetry).

Impedance spectroscopy studies the how the real part of the permittivity of a sample changes with temperature. Close to a phase transition, a sharp peak can be seen, as an abrupt change in the structure and electrical properties of the material is taking place:

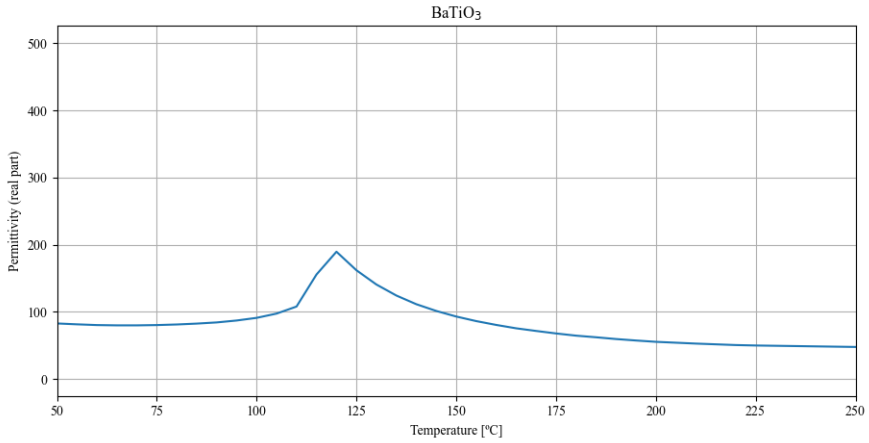

Figure 3.11: Impedance analysis performed on $BaTiO_3$: real part of the permittivity (ϵ') against temperature. $BaTiO_3$ is a strong ferroelectric at room temperature. Observe at 120^{o}C a strong feature. Above this temperature, the material stops behaving as a ferroelectric and enter the paraelectric phase; with a linear response to the external field applied.

Measurements with this technique were trialed but were not conclusive as the apparatus proved to be unstable.

On the other hand, DSC is a measurement technique that detects the adsorption or emission of heat produced during the temperature variation of the sample[26]. The sample, along with a highly inert reference material, is placed in a furnace and subjected to a precisely controlled temperature change. When a thermal transition occurs, the sample either gains or loses energy, depending on whether it is an exothermic or endothermic process, respectively. This reaction heat or enthalpy is measured and serves to detect structural changes in the material[8]. In ferroelectrics, a ferroelectric-to-paraelectric phase transition occurs, which is associated with an endothermic transition. Therefore, this analysis is of particular relevance for locating such transitions.

This measurements were sent to the same scientific facility mentioned before (*SEGAI*), but unfortunately have not arrived in time as the date of this publication

Taking as reference other studies[7], the phase transitions of La-Er compounds would suggest that for $La_{0.85}Er_{1.15}(MoO_4)_3$ and $LaEr(MoO_4)_3$ should be in ferroelectric regime at room temperature. With $La_{1.15}Er_{0.85}(MoO_4)_3$ there is more doubts, but nonetheless, this projects aim is to be able to classify these three compounds and work as basis for further work on similar materials.

4. Results and discussion

En esta sección, se analizan los resultados de las mediciones de histéresis, densidad de corriente y el método PUND para las tres proporciones de la solución sólida $La_{2-x}Er_x(MoO_4)_3$ con x=0.85, 1 y 1.15. Se comparan estos resultados con los perfiles típicos de las muestras de referencia para evaluar el carácter ferroeléctrico de cada proporción. En general, se observa un mayor comportamiento ferroeléctrico en las proporciones $La_{0.85}Er_{1.15}(MoO_4)_3$ y $LaEr(MoO_4)_3$ en comparación con $La_{1.15}Er_{0.85}(MoO_4)_3$. Se realiza un análisis cualitativo y cuantitativo en todas las técnicas para respaldar estas conclusiones. Estos resultados proporcionan información importante sobre las propiedades eléctricas de los materiales.

4.1 Hysteresis

The hysteresis routine was performed for all three of the substances. Several external fields were applied in order to understand the evolution of the cycles with this variable. The measurements were taken at all times with a signal period of 100ms (ν = 10Hz).

The choice of frequency for hysteresis loop measurements depends on the specific characteristics of the material under investigation. Different materials exhibit varying responses at different frequencies due to their inherent properties and polarization dynamics.

For every new compound, trial and error usually works best in finding the optimal range of frequencies for clear results. In our case, our starting point was the one published in [7], where similar proportions of La-Er molibdates were studied: $La_{0.75}Er_{1.25}(MoO_4)_3$, $LaEr(MoO_4)_3$ and $La_{1.25}Er_{0.75}(MoO_4)_3$.

After many attempts, ν = 10Hz showed the most consistent measurements for all three of our compounds. A frequency of 10Hz allows for capturing the polarization dynamics of the material within a reasonable time frame. It provides a balance between capturing the rapid polarization switching behavior of ferroelectric materials and ensuring sufficient data points for accurate analysis.

Furthermore, by using a moderate frequency like 10Hz, the capacitive effects can be minimized, enabling a more accurate characterization of the intrinsic ferroelectric behavior of the La-Er compounds.

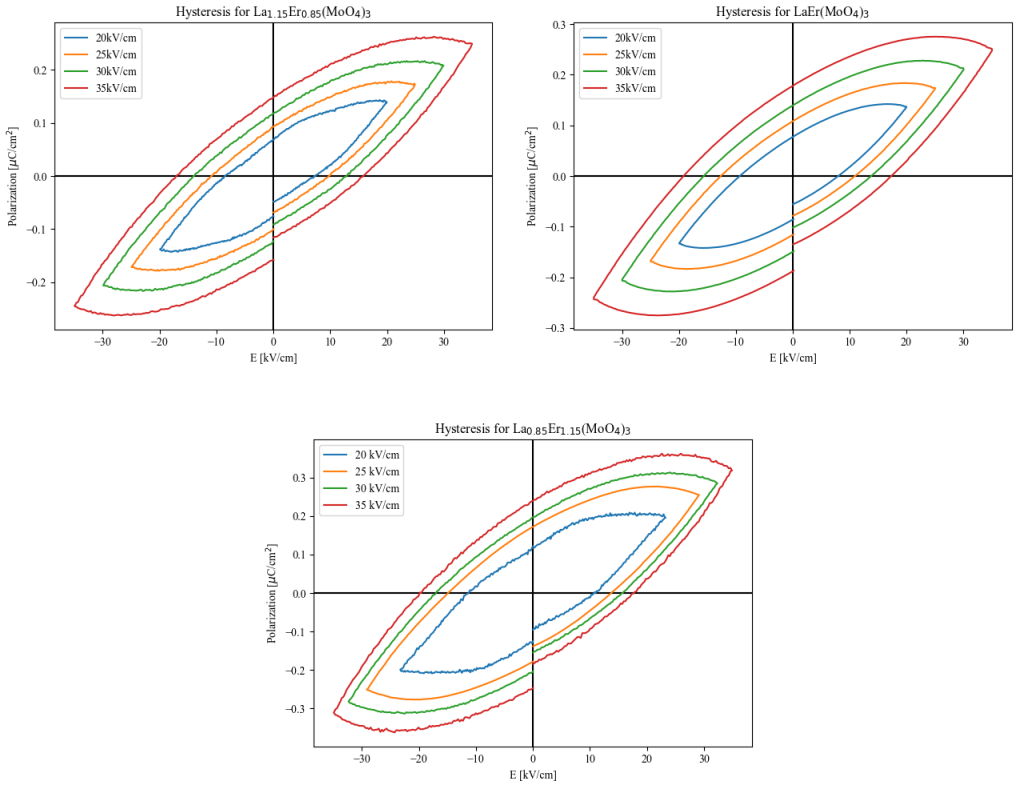

Figure 4.1: Hysteresis cycles at room temperature and at 10Hz for the series $La_{2-x}Er_x(MoO_4)_3$. The maximum applied fields for the three compounds are: 20kV/cm (blue), 25kV/cm (orange), 30kV/cm (green), 35kV/cm (red).

In figure 4.1, the hysteresis loops obtained can be observed. For the mentioned frequency, measurements were taken for maximum voltage values of: 35kV/cm, 30kV/cm, 25kV/cm and 20kV/cm.

A more ferroelectric material will exhibit a larger area inside its hysteresis loop; a direct consequence of the ability of retaining polarization. In most cases, the differences in area con be studied by the naked eye. Regarding this, from our results we can rank from larger to smaller area: $La_{0.85}Er_{1.15}(MoO_4)_3$, $LaEr(MoO_4)_3$ and $La_{1.15}Er_{0.85}(MoO_4)_3$. From this we infer a stronger ferroelectric component as the concentration of Erbium increases. This statement will be also endorsed by a quantitative comparison.

We choose to take a closer look at the 'corners' of the loops (polarization values at maximum external field). These are:

Compound	Electric field (kV/cm)	Polarization (μm/cm^2)
$La_{0.85}Er_{1.15}(MoO_4)_3$	34.945	0.318
$LaEr(MoO_4)_3$	35.025	0.248
$La_{1.15}Er_{0.85}(MoO_4)_3$	34.960	0.237

Table 4.1: Table showing extreme (positive) values for hysteresis profiles (35kV/cm).

Higher polarization values are observed for higher concentration of Erbium, as we would expect from the mentioned earlier. However, both the qualitative and quantitative criteria seem extremely close in $LaEr(MoO_4)_3$ and $La_{1.15}Er_{0.85}(MoO_4)_3$, almost indistinguishable. Neither from the graphs nor from the table we can assume LaEr is more ferroelectric than $La_{1.15}Er_{0.85}(MoO_4)_3$. Clearly, studying hysteresis loops is not enough to classify order this materials in ferroelectric order.

Nonetheless, we can confidently say that none of this compounds is a proper ferroelectric. Comparing with the polarizations values of figure 3.3, La-Er molybdates show an order of magnitude lower to the ones PZT and $BaTiO_3$ exhibit. Still, we do not find a linear response like Teflon in figure 3.4. Already now we are getting hints as to where we can classify our materials, somewhere in between ferroelectrics and dielectrics.

Other measurements will provide further insights on the nature of our compounds.

4.2 Current Density

In similar way, current density measurements were performed. Again, a wide range of frequencies were trialed on the samples, obtaining better results for a higher frequency than in the hysteresis routine. Consequently, measurements were taken for T=10ms (ν = 100Hz).

Due to the small polarization of values of what we assume to be improper ferroelectrics, the intensity of the current is also quite low, even sometimes indistinguishable from noise.

To reduce the effects of this inconvenient, the measurements were taken for the highest electric field possible, since higher currents would be recorded and any kind of phenomena present on the curves would more easily stand out.

As explained earlier, for ferroelectric materials we expect two strong spikes which evidence the inversion of polarization. The results obtained are presented in figure 4.2.

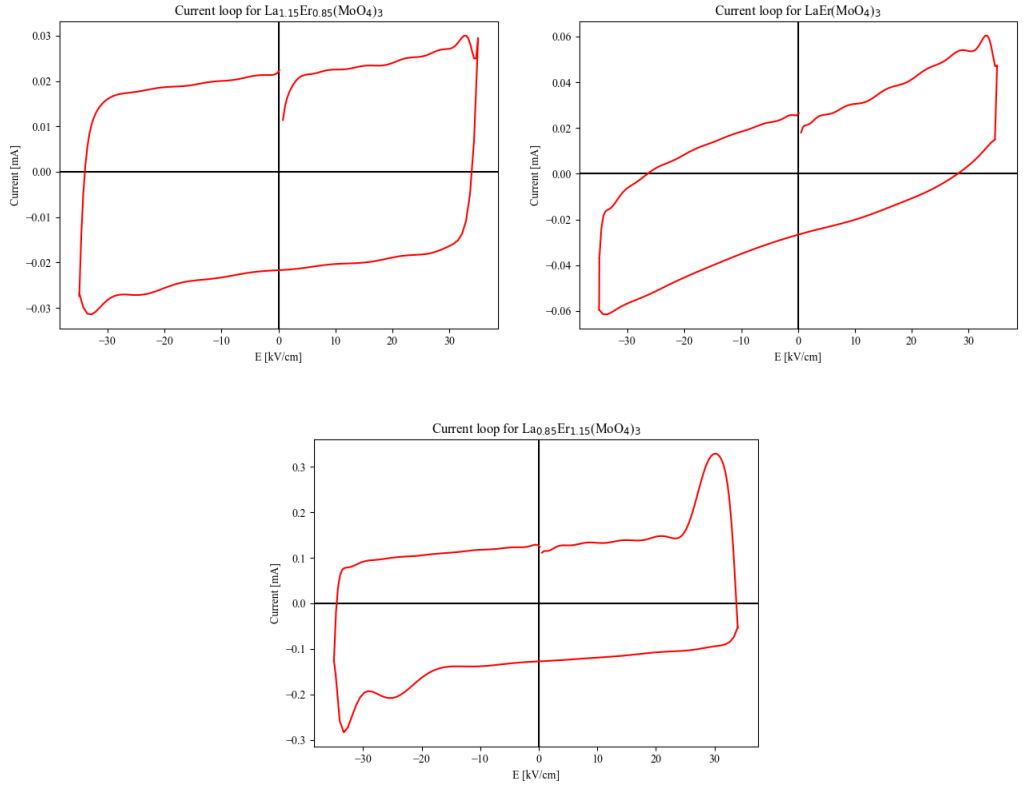

Figure 4.2: Current density loops at room temperature and at 100Hz for the series $La_{2-x}Er_x(MoO_4)_3$. The maximum applied fields for the three compounds was 35kV/cm.

About the results, we can differentiate three different talking points: existence and nature of spikes, shape of the curve and order of magnitude of the data

In our outcome, we can only observe noticeable spikes in $La_{0.85}Er_{1.15}(MoO_4)_3$. The fact that they are symmetrical is crucial, since if they were not, we would immediately deduce that the spikes are not due to inversion of polarization. We can infer that this compound is in ferroelectric regime at room temperature.

As for the other two, spikes are not present, there is a slight hint in both of them but the fact that we find similar features in both of them, suggest the small spikes are related to boundary effects of the measurement equipment rather than to actual ferroelectric phenomena.

On the other hand, we can visibly observe different nature of the curves in all three compounds. Notice how, if we ignore the spikes, $La_{1.15}Er_{0.85}(MoO_4)_3$ and $La_{0.85}Er_{1.15}(MoO_4)_3$ have very similar forms, meanwhile $LaEr(MoO_4)_3$ differentiates some more from the previous two. The $LaEr(MoO_4)_3$ profile may suggest some kind of ferroelectric activity, since for positive electric field we mostly

measure positive current and vice versa. Even though spikes are not visible in this case, we could suggest some polarization inversion as it is not a linear response.

On the other hand, $La_{1.15}Er_{0.85}(MoO_4)_3$ presents a profile which can be considered almost a rectangle. In this case there is nothing that could indicate ferroelectric regime at all.

Finally, we will take a look at the maximum values measured in each case. For the composition $La_{0.85}Er_{1.15}(MoO_4)_3$, the maximum value is around 0.3mA. For $La_{1.15}Er_{0.85}(MoO_4)_3$ 0.03mA and for $LaEr(MoO_4)_3$ around double of this.

Similar conclusions as before can be stated, $La_{0.85}Er_{1.15}(MoO_4)_3$ differentiates from the rest quite clearly, showing stronger ferroelectricity. The other two are again very similar, like the hysteresis loops, showing current density by itself also proofs to be complicated in discerning between them, at least attending to their values. The shape of their curves suggest something but further measurements are required.

Once again, we are able to categorize this materials as something in between ferroelectrics and dielectrics, by comparing them to those from figures 3.7 and 3.8.

4.3 PUND

The interest in subjecting the samples to the PUND routine is gathering extra information related to the remanent component of the global polarization. The pulses allow to almost instantly polarize the samples and, by serving a relaxation time, the 'amount' of domains that remained polarized can be inferred.

This method was carried out in all three compositions, as well as in the previous ferroelectric and dielectric references (namely: PZT, $BaTiO_3$ and Teflon, Al_2O_3). In all cases, the pulse delay was 1s (1000ms) and a pulse width of 1ms.

For the reference samples, the maximum voltage applied was as much as the equipment could take, in order to ensure that they were completely polarized. As to the three La-Er compounds, all evaluations took place for E=30kV/cm, to be able to accurately compare the compounds.

	P^*	P^*_r	P^h	P^h_r	$-P^*$	$-P^*_r$	$-P^h$	$-P^h_r$
PZT	**2.816**	**1.716**	**2.711**	**0.860**	-2.768	-1.501	-2.732	-0.789
$BaTiO_3$	**18.810**	**6.542**	**17.146**	**4.944**	-19.230	-14.440	-16.757	-4.824
$La_{0.85}Er_{1.15}$	**0.241**	**0.056**	**0.241**	**0.048**	-0.243	-0.107	-0.243	-0.096
LaEr	**0.172**	**0.038**	**0.174**	**0.041**	-0.173	-0.039	-0.171	-0.037
$La_{1.15}Er_{0.85}$	**0.126**	**0.020**	**0.126**	**0.019**	-0.126	-0.018	-0.126	-0.018
Teflon	**0.023**	-0.006	**0.023**	-0.001	-0.023	**0.000**	-0.023	**0.001**
Al_2O_3	**0.115**	-0.002	**0.114**	-0.002	-0.116	-0.000	-0.115	**0.001**

Table 4.2: Values obtained when applying the PUND pulses and measuring according to figure 3.9. Notice in bold all positive values.

Relating to figure 3.10, if we want to see something similar to a remanent hysteresis loop, then its a requisite to have P^*, P^*_r, P^h, P^h_r values as positive and $-P^*$, $-P^*_r$, $-P^h$, $-P^h_r$ values as negative.

This condition is clearly satisfied for the ferroelectric references. In this cases, the parameters would sketch out an approximation of the hysteresis loop similar to figure 3.10. Remanent polarization is highly present here as evidenced by the elevated values (wide cycle).

On the other hand, the randomness in the data for the reference dieletrics, indicates no remanent polarization component. In other words, the results show as chaotic since we are trying to measure a feature which simply is not there. When a pulse is applied to this samples, the electric domains briefly align with the direction of the field. However, as soon as there is no more electric activity, the dipoles return to an arbitrary configuration where their directions cancel each other.

The La-Er compounds exhibit a more critical behaviour. All of them follow the same trend as the ferroelectric compounds, however, they do it with much smaller values, as we would expect from what we know from the hysteresis and current loops. Notice as well how the magnitude of the data increases as we go from $La_{1.15}Er_{0.85}(MoO_4)_3$ to $La_{0.85}Er_{1.15}(MoO_4)_3$. Certainly, this has its relation with the hysteresis results, as we are applying the same electric field and the magnitude of the values is related with the width of said cycles. Therefore, we could think, like with the density current loops, from more ferroelectric to less: $La_{0.85}Er_{1.15}(MoO_4)_3$, $LaEr(MoO_4)_3$ and $La_{1.15}Er_{0.85}(MoO_4)_3$.

The presence of remanent polarization in the $La_{0.85}Er_{1.15}(MoO_4)_3$ and $LaEr(MoO_4)_3$ compositions indicates their potential for use in non-volatile memory devices, where the ability to retain information without power is essential.

5. Conclusions and Future Work

Three main experimental procedures have been performed on $La_{2-x}Er_x(MoO_4)_3$ (x=0.85, 1, 1.15) solid solutions, ranging form classic approaches (hysteresis and current loops) to less known measurements (PUND method). The aim is, through the combination of this techniques, differentiate a given sample. This *modus operandi* is highly dependant on comparison with the results if the same experiments for tabulated reference materials (ferroelectrics: PZT and $BaTiO_3$; dielectrics: Teflon and Al_2O_3). In most of this cases, only by taking a look at the hysteresis loops we can infer which category they fall in. However, observing the hysteresis cycle of Al_2O_3 in figure 3.4, one could think it is describing a weak ferroelectric cycle, a hypothesis that gains strength when compared to the results for the same measurement of Teflon; we could think this material is an improper ferroelectric. Here is where the interest of the study resides; by adding complementary measurements like density current analysis (figure 3.8), we can deduce that Al_2O_3 suffers no inversion of polarization at all, meaning there is no ferroelectric behaviour present and the 'hysteresis' cycle observed must correspond to losses caused by, for example, leakage currents. As a final confirmation, PUND routine evidences no remanent polarization in this material.

Following similar reasoning, we can overlap hysteresis and current loops to produce figure 5.1.

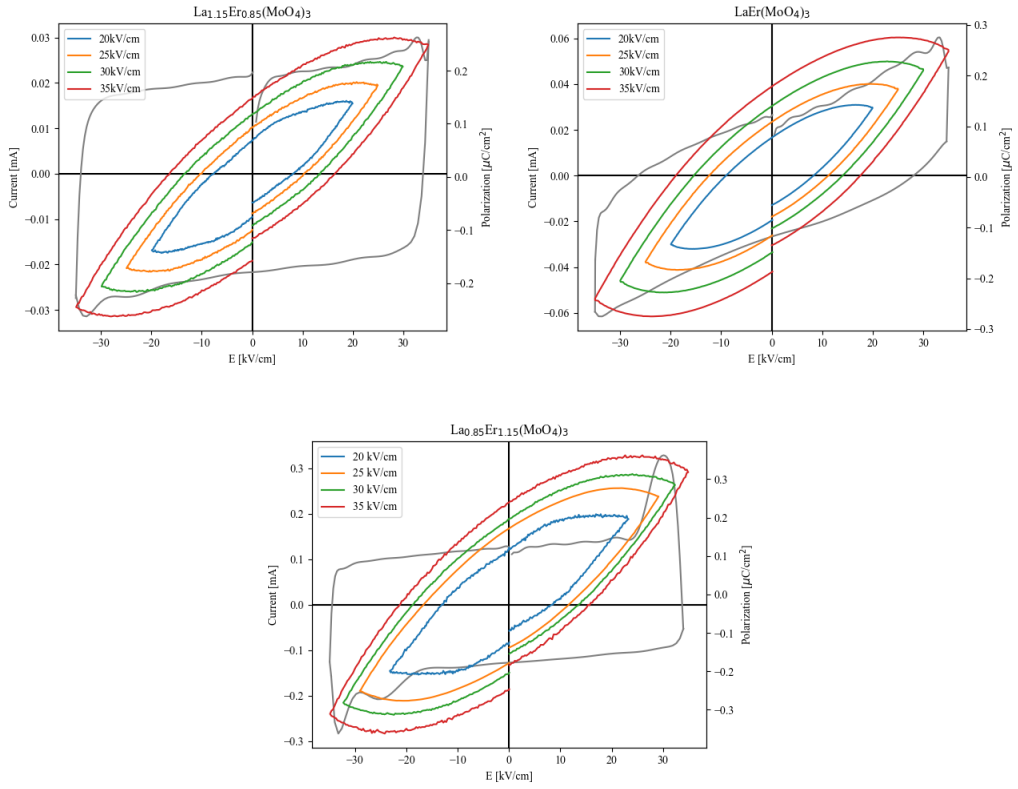

Figure 5.1: Hysteresis cycles and current density loops at room temperature and at 10Hz and 100Hz respectively, for the series $La_{2-x}Er_x(MoO_4)_3$. The maximum applied fields for the three compounds are: 20kV/cm (blue), 25kV/cm (orange), 30kV/cm (green), 35kV/cm (red). Current loop in grey.

On behalf of this results, $La_{0.85}Er_{1.15}(MoO_4)_3$ performs as weak ferroelectric at room temperature. Inversion of polarization clearly takes place. $LaEr(MoO_4)_3$ also partly exhibits this behaviour,

meanwhile $La_{1.15}Er_{0.85}(MoO_4)_3$ is difficult to say whether if its in ferroelectric or paraelectric regime. This last solid solution most probably has its transition temperature very close to room temperature, hence the unclear results over all experiments for this composition.

The introduction of Er into the La-based compound introduces atomic-scale disorder and perturbs the crystal lattice structure. This disruption can lead to the formation of structural defects and local distortions, which can enhance the ferroelectric properties of the material. The presence of Er ions in the crystal lattice may introduce additional polarization sites and contribute to the development of ferroelectric domains.

Furthermore, the substitution of La with Er can alter the overall symmetry and ionic size of the crystal structure. These changes can affect the polarization response and enhance the ferroelectric behavior. The different valence state of Er compared to La may also contribute to the modified electronic structure, resulting in enhanced polarization switching capabilities.

Additionally, the presence of Er can influence the electrical conductivity and charge carrier mobility in the material. These factors can affect the transport of charges during the polarization switching process, leading to a more pronounced ferroelectric response.

As for the aim of the investigation, although there is a notable trend of properties as the composition is gradually changed, further techniques would certainly aid in studying improper ferroelectrics. The order of magnitude of the ferroelectric phenomena in these materials is so low that we can still not say for certain whether a sample is in ferroelectric or paraelectric regime (specially evident with the $La_{1.15}Er_{0.85}(MoO_4)_3$ proportion). However, we have proven that these three techniques are sufficient to differentiate between improper ferroelectrics and dielectrics with losses. This may seem irrelevant but, as mentions in the introduction, there are far too many authors which wrongly assure that certain materials exhibit a ferroelectric hysteresis cycle. In the counterpart, articles could be rejected from publishing as hysteresis loops are understood as leakage current losses. Current loops and PUND can be the backup that investigators exploit to demonstrate their material shows ferroelectric behavior.

With a more flexible timing, phase transition measurements should have been performed after X-Ray diffraction but before the hysteresis, current loops and PUND. Furthermore, a more exhaustive analysis could have been done from the PUND measurements; the parameters hide much more information than what was discussed in this project.

In addition, Radiant Systems provide with another routine called 'Remanent Hysteresis', which uses two different configurations of hysteresis cycles to discern between distinct type of responses; it separates the remanent and non-remanent polarization responses from the inner resistance, linear capacitance and diode effects. This would have been an interesting tool to contribute to the robustness of the model.

Based on the findings and results of this project, there are several potential directions for future work and research. For example, a wider range of La-Er compositions could be explored to gain a more comprehensive understanding of the effects of varying La and Er concentrations on the ferroelectric behavior. More interestingly, not only the ratios of La-Er could be modified, dopants could also be considered.

Moreover, measurements and analysis at different temperature ranges are a natural step to expand the knowledge of the La-Er solid solutions. This could provide insights into phase transitions, Curie temperatures, and the stability of ferroelectric properties over a broader temperature range.

In addition, further comparing the La-Er solid solutions with additional reference materials is key to confirm the understanding of their unique properties. This could involve exploring other ferroelectric and dielectric materials to establish a broader context for their behavior.

A more advanced and thrilling suggestion is to utilize advanced microscopy techniques, such as scanning electron microscopy (SEM) or transmission electron microscopy (TEM), to examine the microstructure and crystal defects within the La-Er solid solutions. Understanding the microstructure can help correlate structural features with the observed ferroelectric properties.

Bibliography

1. *Agate Mortar with Pestle* Auxilab. Available at: https://www.auxilab.es/en/laboratory-equipment/agate-mortar-with-pestle-140-mm/.
2. Aitasalo, M. *et al.* Persistent luminescence phenomena in materials doped with rare earth ions. *J. Solid State Chem.* **171,** 114–122 (2003).
3. *Aluminium oxide* Wikipedia. Available at: https://en.wikipedia.org/wiki/Aluminium_oxide.
4. Atuchin, V. *et al.* Synthesis and spectroscopic properties of monoclinic -Eu2(MoO4)3. *J. Phys. Chem. C* **118,** 15404–15411. https://pubs.acs.org/doi/abs/10.1021/jp5040739 (2014).
5. *Barium titanate* Wikipedia. Available at: https://en.wikipedia.org/wiki/Barium_titanate.
6. Bass, M. COMBINING GRAPHENE AND ORGANIC FERROELECTRIC FOR POSSIBLE MEMORY DEVICES. https://www.researchgate.net/figure/Schematic-representation-of-Sawyer-Tower-hysteresis-loop-measurement-technique-Adapted_fig4_259759119 (2023).
7. Gil de Cos, G. *et al. Unexpected Wide Tuning of Ferroelectric Properties by Varying the Er Concentration in* $La_{2-x}Er_x(MoO_4)_3(x = 0.75, 1, 1.25)$*SolidSolutions* Available at SSRN: https://ssrn.com/abstract=4027267 or http://dx.doi.org/10.2139/ssrn.4027267.
8. Grado en Física. Universidad de La Laguna. *Técnicas de obtención y caracterización de materiales. Tema 2: Análisis Térmico* ().
9. Habouti, S., Solterbeck, C. & Es-Souni, M. Applied Physics Letters. *Appl. Phys. Lett.* **88** (2006).
10. *Inorganic Crystal Structure Database* ICSD. Available in: https://icsd.products.fiz-karlsruhe.de/.
11. Kaczmarek, A. & Van Deun, R. Rare earth tungstate and molybdate compounds–from 0D to 3D architectures. *Chem. Soc. Rev.* **42,** 8835–8848. https://doi.org/10.1039/C3CS60166H (2013).
12. Kaminskii, A. *Laser Crystals: Their Physics and Properties* (Springer Berlin, 2013).
13. *Lead zirconate titanate* Wikipedia. Available at: https://en.wikipedia.org/wiki/Lead_zirconate_titanate.
14. Lee, J.-S., Kang, B. & Jia, Q. Applied Physics Letters. *Appl. Phys. Lett.* **91** (2007).
15. Lüker, A. *Sol-Gel derived Ferroelectric Thin Films for Voltage Tuneable Applications* (VDM Verlag Dr. Müller, 2010).
16. Park, J., Park, J., Jeong, Y. & Jang, H. Applied Physics Letters. *Appl. Phys. Lett.* **91** (2007).
17. *Platinum* Wikipedia. Available at: https://en.wikipedia.org/wiki/Platinum.
18. *Polytetrafluoroethylene* Wikipedia. https://en.wikipedia.org/wiki/Polytetrafluoroethylene.
19. Pust, P., Schmidt, P. & Schnick, W. A revolution in lighting. *Nat. Mater.* **14,** 454–458. https://doi.org/10.1038/nmat4270 (2015).
20. *Radiant Systems* Available at: https://www.ferrodevices.com/.
21. Rodriguez-Carvajal, J. & Team, T. F. *Fullprof suite* Available in: http://www.fullprof.org/.
22. Saidi, K. & Dammark, M. Upconversion luminescence and optical temperature sensing characteristics of Er^{3+}/Yb^{3+}*codoped*$Na_3Gd(PO_4)_2$*phosphors*. *J. Solid State Chem.* **300,** 122214. https://doi.org/10.1016/j.jssc.2021.122214 (2021).
23. Scott, J. F. J. Phys.: Condens. Matter. **20** (2008).
24. Smets, B. Phosphors based on rare-earths, a new era in fluorescent lighting. *Mater. Chem. Phys.* **16,** 283–299. https://doi.org/10.1016/0254-0584(87)90103-9 (1987).
25. Su, W. *et al.* Applied Physics Letters. *Appl. Phys. Lett.* **91** (2007).

26. TA Instruments-Waters LLC. *Simultaneous Thermal Analyzer. Discovery STD Getting started guide* Revision A. TA Instruments-Waters LLC (May 2017).

27. Valasek, J. Piezoelectric and Allied Phenomena in Rochelle Salt. *Physical Review* **15,** 537–538 (1920).

28. Van Krevel, J., van Rutten, J., Mandal, H., Hintzen, H. & Metselaar, R. Luminescence properties of terbium-, cerium-, or europium-doped α-sialon materials. *J. Solid State Chem.* **165,** 19–24. https://doi.org/10.1006/jssc.2001.9484 (2002).

29. Xia, W. *et al.* Tuning of crystal phase and luminescence properties of $Gd_2(MoO_4)_3 : Dy^{3+}$ *phosphors*. *Mater. Res. Bull.* **47,** 2535–2540. https://doi.org/10.1016/j.materresbull.2012.05.003 (2012).

30. Xu, L., Lu, C., Zhang, Z., Yang, X. & Hou, W. Various self-assembled three-dimensional hierarchical architectures of La2(MoO4)3: controlled synthesis, growth mechanisms, luminescence properties and adsorption activities. *Nanoscale* **2,** 995–1005. https://doi.org/10.1039/B9NR00392D (2010).

31. Yuan, G., Yang, Y. & Siu, W. Applied Physics Letters. *Appl. Phys. Lett.* **91** (2007).

Appendix

Mass of each compound used in all solid state reactions.

	Reactants		Product
Compound	Er_2O_3	$3MoO_3$	$Er_2(MoO_4)_3$
Mol. mass [g/mol]	382.52	431.82	814.39
Mass needed [g]	0.4697	0.5302	1
+10% [g]	0.5167	0.5832	1.1

Table 5.1: $Er_2O_3 + 3MoO_3 \rightarrow Er_2(MoO_4)_3$
4 pellets obtained

	Reactants		Product
Compound	La_2O_3	$3MoO_3$	$La_2(MoO_4)_3$
Mol. mass [g/mol]	325.82	431.82	757.64
Mass needed [g]	0.8601	1.1399	2
+10% [g]	0.9461	1.2539	2.2

Table 5.2: $La_2O_3 + 3MoO_3 \rightarrow La_2(MoO_4)_3$
5 pellets obtained

	Reactants		Product
Compound	$La_2(MoO_4)_3$	$Er_2(MoO_4)_3$	$2LaEr(MoO_4)_3$
Mol. mass [g/mol]	757.6238	814.3328	1571.9566
Mass needed [g]	0.2410	0.2590	0.5
+10% [g]	0.2650	0.2849	0.55

Table 5.3: $La_2(MoO_4)_3 + Er_2(MoO_4)_3 \rightarrow 2LaEr(MoO_4)_3$
2 pellets obtained

	Reactants		Product
Compound	$(23/40)\cdot La(MoO_4)_3$	$(17/40)\cdot Er_2(MoO_4)_3$	$La_{1.15}Er_{0.85}(MoO_4)_3$
Mol. mass [g/mol]	435.6337	346.0914	781.7237
Mass needed [g]	0.2786	0.2214	0.5
+10% [g]	0.3065	0.2435	0.55

Table 5.4: $1.15\cdot La_2(MoO_4)_3 + 0.85\cdot Er_2(MoO_4)_3 \rightarrow 2La_{1.15}Er_{0.85}(MoO_4)_3$
2 pellets obtained

	Reactants		Product
Compound	$(17/40)\cdot La(MoO_4)_3$	$(23/40)\cdot Er_2(MoO_4)_3$	$La_{0.85}Er_{1.15}(MoO_4)_3$
Mol. mass [g/mol]	321.9901	468.2414	790.2315
Mass needed [g]	0.2037	0.2963	0.5
+10% [g]	0.2241	0.3259	0.55

Table 5.5: $0.85\cdot La_2(MoO_4)_3 + 1.15\cdot Er_2(MoO_4)_3 \rightarrow 2La_{0.85}Er_{1.15}(MoO_4)_3$
2 pellets obtained